Insights into the conservation and diversification of the molecular functions of YTHDF proteins

Short title: Diversification of YTHDF proteins in land plants

Daniel Flores-Téllez[1,2], Mathias Due Tankmar[1], Sören von Bülow[1], Junyu Chen[1], Kresten Lindorff-Larsen[1], Peter Brodersen[1]* and Laura Arribas-Hernández[1]*

[1] University of Copenhagen, Biology Department. Ole Maaløes Vej 5, 2200 Copenhagen N, Denmark.
[2] Universidad Francisco de Vitoria, Facultad de Ciencias Experimentales. Ctra. Pozuelo-Majadahonda km 1800, 28223 Pozuelo de Alarcón (Madrid), Spain.

*Corresponding authors

Email pbrodersen@bio.ku.dk (P.B.) and laura.arribas@bio.ku.dk (L.A.-H.)

The authors declare that they have no conflict of interest

Abstract

YT521-B homology (YTH) domain proteins act as readers of *N6*-methyladenosine (m^6A) in mRNA. Members of the YTHDF clade determine properties of m^6A-containing mRNAs in the cytoplasm. Vertebrates encode three YTHDF proteins whose possible functional specialization is debated. In land plants, the YTHDF clade has expanded from one member in basal lineages to eleven so-called EVOLUTIONARILY CONSERVED C-TERMINAL REGION1-11 (ECT1-11) proteins in *Arabidopsis thaliana*, named after the conserved YTH domain placed behind a long N-terminal intrinsically disordered region (IDR). *ECT2*, *ECT3* and *ECT4* show genetic redundancy in stimulation of primed stem cell division, but the origin and implications of YTHDF expansion in higher plants are unknown, as it is unclear whether it involves acquisition of fundamentally different molecular properties, in particular of their divergent IDRs. Here, we use functional complementation of *ect2*/*ect3*/*ect4* mutants to test whether different YTHDF proteins can perform the same function when similarly expressed in leaf primordia. We show that stimulation of primordial cell division relies on an ancestral molecular function of the m^6A-YTHDF axis in land plants that is present in bryophytes and is conserved over YTHDF diversification, as it appears in all major clades of YTHDF proteins in flowering plants. Importantly, although our results indicate that the YTH domains of all arabidopsis ECT proteins have m^6A-binding capacity, lineage-specific neo-functionalization of ECT1, ECT9 and ECT11 happened after late duplication events, and involves altered properties of both the YTH domains, and, especially, of the IDRs. We also identify two biophysical properties recurrent in IDRs of YTHDF proteins able to complement *ect2 ect3 ect4* mutants, a clear phase separation propensity and a charge distribution that creates electric dipoles. Human and fly YTHDFs do not have IDRs with this combination of properties and cannot replace ECT2/3/4 function in arabidopsis, perhaps suggesting different molecular activities of YTHDF proteins between major taxa.

Author Summary

Regulation of gene expression is essential to life. It ensures correct balancing of cellular activities and the controlled proliferation and differentiation necessary for the development of multicellular organisms. Methylation of adenosines in mRNA (m^6A) contributes to genetic control, and absence of m^6A impairs embryo development in plants and vertebrates. m^6A-dependent regulation can be exerted by a group of cytoplasmic proteins called YTHDFs. Higher plants have many more YTHDFs than animals, but it is unknown whether these many YTHDF proteins carry out fundamentally different or roughly the same molecular functions, as only a small fraction of them have been studied thus far. This work addresses the origin and reasons behind YTHDF expansion during land plant evolution and reveals that most YTHDFs in flowering plants have the same molecular functions that facilitate rapid division of differentiating stem cells. Remarkably, this molecular activity is present in the most basal lineage of land plants and functions similarly across 450 million years of land plant evolution. We also identified a few plant YTHDF proteins with divergent molecular function despite their ability to bind to m^6A. Our work provides a firm basis for further advances on understanding molecular properties and biological contexts underlying YTHDF diversification.

Introduction

N6-methyladenosine (m^6A) is the most abundant modified nucleotide occurring internally in eukaryotic mRNA. It is of major importance in gene regulation as illustrated by the embryonic lethality of mutants in the dedicated mRNA adenosine methyltransferase in higher plants [1] and in mammals [2]. The presence of m^6A in an mRNA may have multiple biochemical consequences. These include changes in the secondary structure [3-5] and the creation of binding sites for RNA-binding proteins specialized for m^6A recognition [6, 7]. YT521-B homology (YTH) domain proteins [8] constitute the best studied class of m^6A-binding proteins [6, 7, 9]. They achieve specificity for m^6A via an aromatic pocket accommodating the *N6*-adenosine methyl group, such that the affinity of isolated YTH domains for m^6A-containing RNA is 10-20-fold higher than for unmodified RNA [9-14].

Two different phylogenetic clades of YTH domains have been defined, YTHDC and YTHDF, sometimes referred to simply as DC and DF [6, 15]. Genetic studies show that major functions of m^6A in development in both vertebrates and higher plants depend on the YTHDF clade of readers [16-22]. In all cases studied in detail thus far, plant and animal YTHDF proteins are cytoplasmic in unchallenged conditions [15, 16, 23-26], and contain a long N-terminal intrinsically disordered region (IDR) in addition to the C-terminal YTH domain [6, 8, 27]. While the YTH domain is necessary for specific binding to m^6A in mRNA [9-14], the IDR is considered to be the effector part of the protein [9, 28-30]. Nonetheless, it has been proposed that the IDR may also participate in RNA binding, because the YTH domain alone has low affinity for mRNA [6]. Indeed, the IDR-dependent crosslinks between a YTHDF protein and mRNA detected upon UV-irradiation of living arabidopsis seedlings [31] experimentally supports such a mechanism, conceptually equivalent to the contribution of IDRs in transcription factors to specific DNA binding [32]. Additionally, the IDR may be involved in phase separation. Plant YTHDF proteins can form condensates *in vitro* [16] and, upon stress, localize *in vivo* to distinct foci [16, 26] identified as stress granules [26]. Similar properties have been reported for human YTHDFs, which engage in liquid-liquid phase separation when concentrated on polyvalent m^6A-modified target RNA *in vitro* [33-36].

While yeast, flies and primitive land plants encode only one YTHDF protein [24-26, 37, 38], vertebrates have three closely related paralogs (YTHDF1-3) [6, 8, 15, 39] and higher plants encode an expanded family, with eleven members in *Arabidopsis thaliana* (*Ath*) referred to as EVOLUTIONARILY CONSERVED C-TERMINAL REGION1-11 (ECT1-11) [27, 40]. It is a question of fundamental importance for the understanding of how complex eukaryotic systems use the regulatory potential of m^6A whether these many YTHDF proteins perform the same biochemical function, or whether their molecular properties are specialized. Such molecular specialization could, for instance, arise as a consequence of differential binding specificity to mRNA targets, distinct protein-protein interaction properties,

83 or distinct biophysical properties of IDRs, such as those related to the propensity to phase
84 separate [41, 42]. Alternatively, diversification of biological functions could be achieved with
85 distinct expression patterns or induction by environmental cues, even if targets and
86 molecular functions are the same. The studies on YTHDF specialization in vertebrate cells
87 illustrate the importance of the topic, and, equally, the importance of addressing it rigorously
88 [43]. Initial work on mammalian cell cultures advocated a model in which YTHDF1 would
89 enhance translation of target mRNAs, YTHDF2 would promote mRNA decay, and YTHDF3
90 would be able to trigger either of the two [9, 44-46]. Nonetheless, subsequent research work
91 in mouse, zebrafish and human cell culture involving single and combined *ythdf* knockouts
92 and analysis of interacting mRNAs and proteins [18, 22, 39], and comparative studies of
93 human YTHDF1/2/3 structure and molecular dynamics [47] do not support functional
94 specialization, and propose a unified molecular function for all three vertebrate YTHDFs in
95 accelerating mRNA decay. Whether metazoan YTHDF1/2/3 are molecularly redundant or
96 not, and what their precise molecular functions may be, are topics that continue to be
97 debated as of today [48].
98 The great expansion of YTHDF proteins in higher plants is unique among eukaryotes
99 [8]. Phylogenetic analyses of plant YTHDF domains have established the existence of 3
100 clades in angiosperms, DF-A (comprising *Ath* ECT1, ECT2, ECT3, ECT4), DF-B
101 (comprising *Ath* ECT5, ECT10, ECT9), and DF-C (comprising *Ath* ECT6, ECT7, ECT8 and
102 ECT11) [26]. The fact that the eleven arabidopsis paralogs have the aromatic residues
103 necessary for specific binding to m^6A [49] suggests that they may all function as m^6A
104 readers. The unified model for YTHDF function recently proposed for the three vertebrate
105 paralogs [18, 22, 39] is consistent with what had already been established for *Ath* ECT2,
106 ECT3 and ECT4 in the plant DF-A clade [16], even though the three plant paralogs are more
107 divergent in sequence than the highly similar mammalian YTHDF1-3 [8, 16, 39]. The two
108 most highly expressed members in *A. thaliana*, ECT2 and ECT3, accumulate in dividing
109 cells of organ primordia and exhibit genetic redundancy in the stimulation of stem cell
110 proliferation during organogenesis [16, 17]. The two proteins probably act truly redundantly
111 *in vivo* to control this process, because they associate with highly overlapping target sets in
112 wild type plants, and each exhibits increased target mRNA occupancy in the absence of the
113 other protein [23]. Simultaneous knockout of *ECT2* and *ECT3* causes a 2-day delay in the
114 emergence of the first true leaves, aberrant leaf morphology, slow root growth and defective
115 root growth directionality among other defects [16, 17] that resemble those of plants with
116 diminished m^6A deposition [50-52]. For the third DF-A clade member, *ECT4*, the genetic
117 redundancy is only noticeable in some tissues as an exacerbation of *ect2/ect3* phenotypes
118 upon additional mutation of *ECT4*, most conspicuously seen in leaf morphogenesis [16, 17].
119 Despite the strong evidence for redundant functions among these three YTHDF paralogs in

120 the DF-A clade, the presence of many other YTHDF proteins in arabidopsis leaves open the
121 question of whether substantial functional specialization of YTHDF proteins exists in plants.
122 In this study, we systematically define overlaps in the molecular functions of YTHDF
123 proteins in land plants (embryophytes). Employing functional complementation of leaf
124 formation in triple *ect2/ect3/ect4* (*te234*) mutants, we demonstrate that at least one member
125 of all clades in arabidopsis, and the only YTHDF protein from a group of primitive land
126 plants, can replace ECT2/3/4 functions. In contrast, a few late-diverging ECTs were not able
127 to perform the molecular functions of ECT2/3/4. Based on these results, we propose an
128 ancestral molecular role of land plant YTHDF proteins in stimulation of primordial cell
129 proliferation, and sustained functional redundancy during the diversification process that
130 started more than 400 million years ago (Mya). In addition, our results also support the
131 functional divergence of a small subset of fast-evolving plant YTHDF proteins with
132 contributions to specialization mainly from the IDRs, but also from the YTH domains.
133
134 **Results**
135 *The phylogeny of YTHDF proteins comprises several clades in land plants*
136 The adaptation of plants to terrestrial life was accompanied by the acquisition of
137 morphological, physiological, and genomic complexity [53-55]. Knowing how diversification
138 of YTHDF proteins came about during the course of plant evolution is relevant to understand
139 their distinct functions and may hint at roles they might have played in this process.
140 However, the species included in the so far most detailed phylogenetic study on plant
141 YTHDF proteins jump from bryophytes (mosses, liverworts and hornworts [54, 56-60]) to
142 angiosperms (flowering plants) [26]. To include the YTHDF repertoires of intermediately
143 diverging clades of embryophytes such as lycophytes, ferns, and gymnosperms, we
144 performed phylogenetic analyses using YTHDF proteins from 32 species widely spread
145 across land plant evolution. We also included YTHDFs from 8 species of green algae
146 (chlorophytes and charophytes) and, as outgroup, 3 microalgal species from eukaryotic taxa
147 evolutionarily close to plants (Fig 1A). In the resulting phylogenetic tree, all embryophyte
148 YTHDFs branch from a single stem that connects this monophyletic group to the more
149 divergent green algal orthologs (Figs 1B and S1-S3), whose peculiarities are further
150 considered in the discussion. Regarding land plants, the tree largely agrees with the DF-
151 A/B/C clades defined on the basis of angiosperm YTHDF sequences [26], with some minor
152 differences. We consider that the former DF-C group comprising *Ath* ECT6/7/8/11 [26] can
153 be subdivided into two groups that diverged early during YTHDF radiation (Figs 1B and S1).
154 Thus, we introduced the name 'DF-D' for the clade defined by one *Amborella trichopoda* (a
155 basal angiosperm) YTHDF protein (*Atr* DFD) and *Ath* ECT6/7 (Figs 1B and S1).

Furthermore, since the group comprising bryophyte YTHDFs did not receive a designation in previous studies, we named it DF-E (mnemotechnic for 'Early'). It includes YTHDF proteins from bryophytes and some lycophyte orthologs that branched close to the moss subgroup (Figs 1B and S1). Finally, an additional group composed of YTHDF proteins from six species of ferns and two gymnosperms was named DF-F, as they did not fall into any of the other clades (Figs 1B and S1). Interestingly, the alignment revealed independent gains and losses of molecular traits during plant YTHDF evolution. For example, an aspartate-to-asparagine substitution in helix α1 that increases affinity for m^6A [61], characteristic of DC and plant DF-B YTH domain proteins [26, 61], is also present in the fern proteins of the DF-F clade, but absent in DF-Es, DF-As and gymnosperm DF-Fs (Fig S4), suggesting independent losses or acquisitions. Taking these observations together, we conclude that land plant YTHDFs are phylogenetically more diverse than previously appreciated.

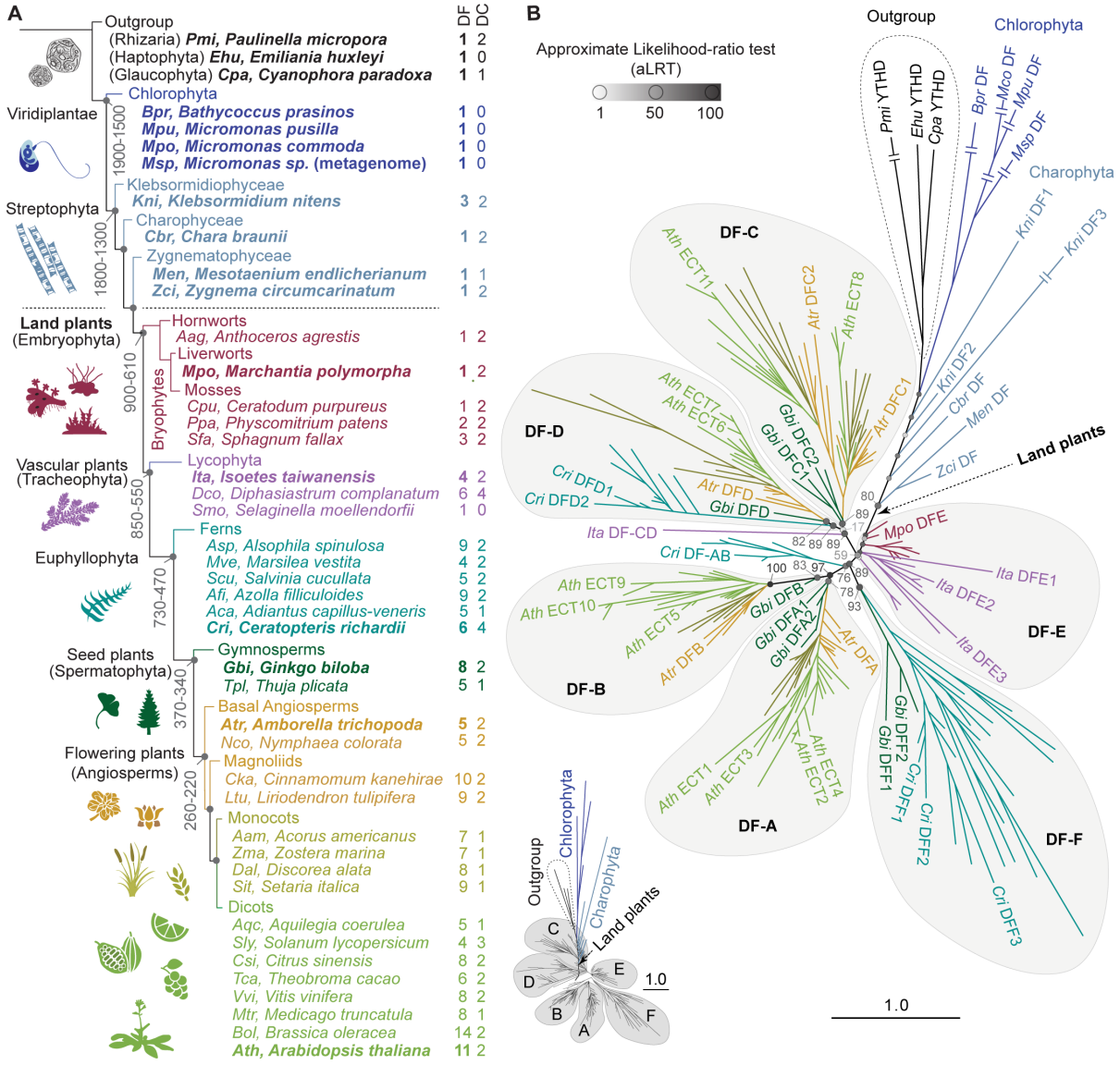

Fig 1. Phylogenetic analysis of YTHDF proteins in plants. (A) Schematic representation of Viridiplantae evolution and relative position of the species used in this study. The architecture of the

171 diagram and the age (million years, My) indicated on some nodes are a simplified version of the trees
172 from Su et al. [59] and Bowman [62]. The length of the branches has been adjusted for illustrative
173 purposes. **(B)** Phylogenetic tree of YTHDF proteins in plants (S1-S4 Datasets), with color-coding and
174 abbreviations of species names as in A. Three YTHDF proteins from taxa outside but evolutionarily
175 close to Viridiplantae are included as outgroup. *Arabidopsis thaliana* (*Ath*) YTHDF proteins are named
176 after the original nomenclature for proteins containing an Evolutionarily Conserved C-Terminal Region
177 (ECT) established by Ok et al. [40]. Proteins from other plant species adhere to the nomenclature
178 established by Scutenaire et al. [26], with small variations reflecting additional clades (DF-E, -F) and
179 the split of the original DF-C clade into -C and -D. Statistical support is calculated as approximate
180 likelihood-ratio test (aLRT), and indicated by grayscale-coded spheres and values on the most
181 relevant nodes. For simplicity, only a subset of proteins is labelled–those from one representative
182 species of the main taxa highlighted in bold in A–, but a comprehensive representation of the same
183 tree with all protein names and aLRT values is available in S1 Fig. The length of the branches
184 represents the evolutionary distance in number of amino acid substitutions per site relative to the
185 scale bar. Double lines crossing the longest branches indicate that the branch has been collapsed
186 due to space problems, but a schematic representation of their relative lengths is shown on the lower-
187 left corner, and not-collapsed branches can be found in S1 Fig.
188

189 *YTHDF protein diversification occurred early during land plant evolution*

190 Our phylogenetic analysis shows that plant YTHDF diversification started at least before the
191 radiation of Euphyllophytes (plants with true leaves comprising ferns, gymnosperms and
192 angiosperms) more than 410 Mya [59, 63]. This is because bryophytes possess one or two
193 YTHDFs in the 'early clade' (DF-E), while all six fern species analyzed here have extended
194 sets DF proteins (4-9 paralogs) that spread into clades DF-F, DF-D, and the branch
195 sustaining the DF-A and DF-B groups (Fig 1B). Furthermore, because one DF-protein from
196 the lycophyte *Isoetes taiwanensis* branches from the common stem between clades DF-C
197 and DF-D (*Ita* DF-CD), it is likely that a first diversification event started in the ancestral
198 vascular plants. Thus, our analysis reveals that YTHDF radiation started early in land plant
199 evolution and coincided with the acquisition of morphological complexity and the adaptation
200 to diverse environments.
201

202 *A functional complementation assay for plant YTHDF proteins*

203 To address the degree of functional specialization among plant YTHDF proteins in a simple
204 manner, we set up a functional complementation assay that scores the ability of each of the
205 eleven arabidopsis YTHDF proteins (Fig 2A) to perform the molecular functions of ECT2/3/4
206 required for rapid cellular proliferation in leaf primordia. Initial attempts at using the *ECT2*
207 promoter for ectopic *ECT* expression in primordial cells were unsuccessful, as pilot
208 experiments with a genomic *ECT4* fragment revealed that its expression was substantially
209 lower than that of a similar *ECT2* genomic fragment when driven by the *ECT2* promoter (S5
210 Fig), perhaps pointing to the presence of internal *cis*-regulatory elements. We therefore
211 turned to the use of *ECT* cDNAs (c*ECT*s) under the control of the promoter of the ribosomal
212 protein-encoding gene *RPS5A/uS7B/US7Y* (At3g11940 [64, 65]), henceforth *US7Yp*, active

in dividing cells [66] in a pattern that resembles the *ECT2/3/4* expression domain [16, 17]. Transformation of the *US7Yp:cECT2-mCherry* construct in *te234* plants resulted in complementation frequencies of ~40-50% among primary transformants, a percentage slightly lower but comparable to that obtained with the genomic *ECT2-mCherry* construct under the control of *ECT2* promoter and terminator regions (*ECT2p:gECT2-mCherry*) [16] (S6A Fig). Free mCherry expressed from a *US7Yp:mCherry* transgene showed no complementation (S6A Fig), as expected. Importantly, the leaf morphology and the pattern of mCherry fluorescence in *US7Yp:cECT2-mCherry* lines was indistinguishable from that of *ECT2p:gECT2-mCherry* (S6B Fig). Hence, we proceeded with expression of cDNAs encoding all of ECT1-11 fused to C-terminal mCherry under the control of the *US7Y* promoter (henceforth ECT1-11) in *te234* mutants (Fig 2B).

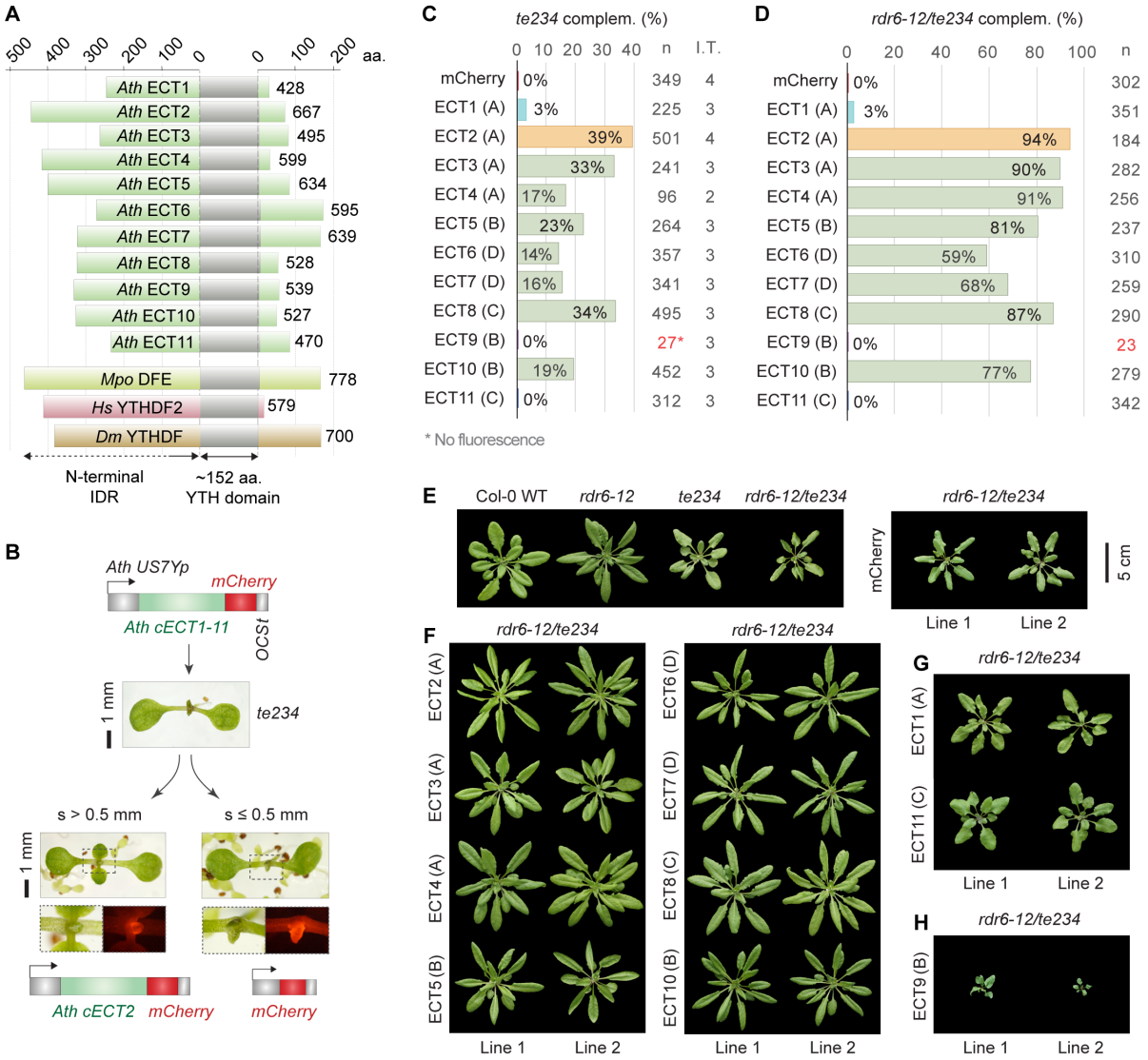

Fig 2. Most but not all arabidopsis YTHDF proteins can replace ECT2/3/4-function. (A) Diagram showing the relative length of the N-terminal IDRs of *Arabidopsis thaliana* (*Ath*) YTHDF proteins (ECT1-ECT11) together with *Marchantia polymorpha* (*Mpo*) DFE, *Homo sapiens* (*Hs*) YTHDF2, and *Drosophila melanogaster* (*Dm*) YTHDF. Numbers indicate the length of the proteins in amino acids

229 (aa). **(B)** Strategy followed for the functional assay. *US7Yp:cECT(X)-mCherry* constructs are
230 introduced in *ect2-1/ect3-1/ect4-2* (*te234*) plants, and complementation rates are estimated by the
231 percentage of primary transformants (T1) whose first true leaves have a size (s) exceeding 0.5 mm
232 after 10 days of growth. The *construct US7Yp:mCherry* is used as negative control. Examples of T1
233 seedlings expressing control and ECT2 constructs are shown. Dashed outlines are magnified below
234 to show mCherry fluorescence in emerging leaves. **(C)** Weighed averages of the complementation
235 percentages observed for each *US7Yp:cECT(X)-mCherry* construct in 2-5 independent
236 transformations (I.T.). Letters between parenthesis indicate the DF- clade assigned to each protein.
237 Colouring highlights ECT2 (reference) and proteins with low or negligible complementation capacity
238 (ECT1/9/11) for fast identification along the manuscript. Low transformation efficiency (T.E.) for ECT9
239 can be inferred by the low number of transformants (n) highlighted in red, but detailed T.E. and raw
240 complementation rates in each transformation can be found in S9 and S7A Figs respectively.
241 Additional data regarding this assay is shown in S8 Fig. **(D)** Same as C on a single transformation
242 using the *rdr6-12/te234* background. **(E-H)** Rosette phenotype of 32-day old T1s bearing
243 *US7Yp:cECT(X)-mCherry* constructs in the *rdr6-12/te234* background, sorted according to their
244 degree of complementation in three panels: F (high), G (residual) and H (non-complementation and
245 enhancement). Different genetic backgrounds and control transformants (mCherry) are shown in *E* as
246 a reference. The scalebar (5 cm) applies to all plants in the four panels.
247
248 *Percentage of complementation among primary transformants as a readout for functionality*
249 To design the experimental approach in detail, we considered the fact that expression of
250 transgenes involves severe variations in levels and patterns among transformants. This is
251 due to positional effects of the T-DNA insertion and the propensity of transgenes to trigger
252 silencing in plants [67], and explains why only a fraction of *ECT2-mCherry* lines rescues loss
253 of ECT2 function (S6A Fig, [16]). Hence, many independent lines need to be analyzed
254 before choosing stable and representative lines for further studies. Taking this into account,
255 we decided to perform systematic and unbiased comparisons of ECT functionality by
256 counting the fraction of primary transformants (henceforth T1s) able to complement the late
257 leaf emergence of *te234* plants for each construct. We set a size threshold for the rapid
258 assessment of large numbers of transformants considering that leaves longer than 0.5 mm
259 after 10 days of growth constitute unambiguous sign of complementation, because this is the
260 minimum size never reached by *te234* or control lines (S2B Fig). Hence, we calculated
261 complementation percentages as the number of T1s with leaf size (s) larger than 0.5 mm
262 relative to the total number of transformants, and averaged that score over several
263 independent transformations (Figs 2C and S7A, S8A).
264
265 *Most arabidopsis YTHDF paralogs can perform the molecular function required for leaf*
266 *development*
267 The results of the comparative analysis reveal a high degree of functional overlap within the
268 arabidopsis YTHDF family, because eight out of the eleven YTHDF proteins, namely
269 ECT2/3/4/5/6/7/8/10, complement the delayed leaf emergence of *ect2/3/4* mutants with
270 frequencies ranging from 14% (ECT6) to 39% (ECT2) when expressed in the same cells

271 (Fig 2C). Importantly, complementation is indirect proof of m^6A-binding ability, because the
272 proteins must bind to the targets whose m^6A-dependent regulation is necessary for correct
273 leaf organogenesis in order to restore ECT2/3/4 function [16]. This conclusion is not trivial,
274 as some eukaryotes lacking canonical m^6A-methyltransferases encode YTH domain proteins
275 [68] and, indeed, the YTH domain of fission yeast Mmi1 does not bind to m^6A [69]. Thus,
276 most, but not all, arabidopsis YTHDF proteins retain the molecular functions required to
277 stimulate proliferation of primed stem cells. Of the three remaining proteins, ECT1 showed
278 only residual complementation capacity, while no complementation was observed for ECT11
279 at this stage (Fig 2C). Finally, we could not conclude at this point whether ECT9 could
280 replace ECT2/3/4 function or not, because this transgene produced very few transformants
281 in the *te234* background with barely visible fluorescence (Figs 2C and S7-S9). All such
282 transformants underwent complete silencing in the following generation (T2).
283
284 *Differences in complementation scores are not explained by a bias in expression levels*
285 Our T1 scoring method relies on the assumption that the *US7Y* promoter drives similar
286 ranges of expression of the different *ECT* cDNAs. However, different silencing propensities
287 between the *ECT* cDNAs might introduce bias in the results. To take this possibility into
288 account, we first performed western blotting from three lines per transgene selected as the
289 best-complementing in their group (S8B Fig). The results showed that the higher
290 complementation scores of e.g. ECT2, ECT3 and ECT8 are not explained by higher
291 expression. Rather, the reverse was true. For example, while ECT2 could complement *te234*
292 plants with the lowest expression among all ECTs, the few lines expressing ECT1 able to
293 pass the complementation threshold had the highest expression of all ECTs, suggesting that
294 ECT1 can only partially compensate for loss of ECT2/3/4 when overexpressed.
295
296 *The same functional classes of ECTs emerge from complementation of silencing-deficient*
297 *te234*
298 Next, we tested whether the same results could be reproduced in plants lacking *RNA-*
299 *DEPENDENT RNA POLYMERASE 6* (*RDR6*), a gene essential for the biogenesis of
300 transgene-derived short interfering RNAs (siRNAs) [70, 71]. Because siRNA-guided
301 transgene silencing is impaired in *rdr6* mutants, higher and more homogenous ranges of
302 expression among different transgenes can be expected in this background. Hence, we
303 constructed *rdr6-12/te234* mutants that exhibited both the narrow, downward-curling leaf
304 phenotype of *rdr6* mutants [72] and the characteristic rosette morphology of *te234* [16]
305 (S10A Fig). Importantly, the delay in leaf emergence was identical in *te234* and *rdr6-*
306 *12/te234* mutants (S10A Fig) and the complementation rates of *ECT2* transgenes were
307 much higher in the silencing-deficient plants (S6A Fig), indicating that the <100%

308 complementation frequencies in *te234* were indeed due to RDR6-dependent silencing. In the
309 *rdr6*/*te234* background, complementation scores of the eight functionally equivalent ECTs
310 (ECT2/3/4/5/6/7/8/10) ranged from 59% (ECT6) to 94% (ECT2), and the differences
311 between these ECTs were less pronounced, but followed a trend largely unchanged
312 compared to the *te234* background (Fig 2C,D). On the other hand, the difference between
313 the eight ECTs with ECT2/3/4-like function and the group of ECTs with negligible
314 complementation capacity (ECT1/9/11) was highlighted by the *rdr6* mutation: ECT1 and
315 ECT11 did not increase their scores (Fig 2D), and absence of silencing resulted in a number
316 of *ECT9* transformants with visible mCherry fluorescence, yet no complementation activity
317 (Figs 2D and S10B), thus verifying the lack of ECT2/3/4-like function of ECT9.
318
319 *Rosette phenotypes corroborate the complementation scores*
320 To verify the results of the complementation assay in the adult phenotype, we characterized
321 rosettes of two independent lines for each transgene (Fig 2E-H). As expected, *rdr6-12/te234*
322 plants expressing ECTs with high complementation scores resembled single *rdr6-12*
323 mutants (Fig 2E,F), while the ECT1 and ECT11 transformants with the biggest first true
324 leaves at 10 DAG produced plants only slightly bigger than the *rdr6-12/te234* background
325 (Fig 2E,G), indicating low but residual ECT2/3/4-like function for these two proteins.
326 Strikingly, *rdr6-12/te234* plants expressing ECT9 exhibited strong developmental
327 phenotypes (Figs 2H and S10B) that resembled those of severely m^6A-depleted plants [51,
328 52]. Such an effect was not observed for any other *Ath* ECT. This result suggests that ECT9
329 can bind to m^6A targets, either exerting opposite molecular actions compared to ECT2/3/4,
330 or simply precluding their possible regulation by remaining ECTs such as ECT5/6/7/8/10 by
331 competitive binding. We tested whether ECT9 can outcompete endogenous ECT2/3/4 in the
332 proliferating cells of the apex by expressing the ECT9 transgene in single *rdr6-12* mutant
333 plants. We found no evidence for this, because the transformation produced many
334 fluorescent T1s without obvious defects (S11 Fig). Altogether, our results indicate that
335 arabidopsis YTHDF proteins may be divided into three functional classes, i)
336 ECT2/3/4/5/6/7/8/10 with the molecular functionality of ECT2/3/4 required for correct and
337 timely leaf formation; ii) ECT1/11, with only residual ECT2/3/4 functions, and iii) ECT9,
338 unable to perform such functions and toxic when present in the expression domain of
339 ECT2/3/4 in their absence.
340
341 *Validation of the functional assay by loss-of-function genetic analysis*
342 One of the predictions on genetic interactions between *Ath ECT* genes that emerges from
343 our results is particularly unexpected and, therefore, suitable for the validation of our
344 complementation assay by classical genetic analysis: Mutation of *ECT1* should not

345 exacerbate the developmental defects of *te234*, even if it is endogenously expressed in leaf
346 primordia. *ECT1* lends itself well to validation for two reasons. First, ECT1 is the closest
347 paralog of ECT2/3/4 (Fig 1B), intuitively suggesting some degree of genetic redundancy.
348 Second, *ECT1* promoter-reporter fusions [40] and mRNA-seq data ([73], S12 Fig) suggest
349 that expression levels and tissue specificity of *ECT1* are comparable to that of *ECT4*, whose
350 activity is easily revealed as an enhancer mutant of *ect2/ect3* [16].
351
352 *ECT1 and ECT2/3/4 are cytoplasmic and are expressed in the same cell types*
353 We first assessed the expression pattern and subcellular localization of ECT1 using stable
354 transgenic lines expressing TFP translationally fused to the C-terminus of *ECT1* (*ECT1-TFP*,
355 S13A Fig). The pattern of turquoise fluorescence was strongly reminiscent of that of
356 fluorescent ECT2/3/4 fusions [16] with signal at the base of young leaves, in leaf primordia,
357 main root tips and lateral root primordia at different stages (Fig 3A-D). In addition, confocal
358 microscopy of meristematic root cells showed cytoplasmic ECT1-TFP signal with
359 heterogenous texture similar to ECT2/3/4 [16] (Fig 3E). We noticed, however, that most root
360 tips had a few cells containing distinct ECT1-TFP foci (Fig 3F) in the absence of stress. We
361 found no trace of free TFP that could be causing imaging artifacts (S13A Fig) but note that
362 the *ECT1-TFP* transgenic lines selected on the basis of visible and reproducible pattern of
363 fluorescence may overexpress *ECT1* (S13B Fig). We conclude from the similar expression
364 pattern and subcellular localization of ECT1 and ECT2/3/4 that assessment of the possible
365 exacerbation of *te234* phenotypes by additional loss of *ECT1* function is a meaningful test of
366 our functional assay.

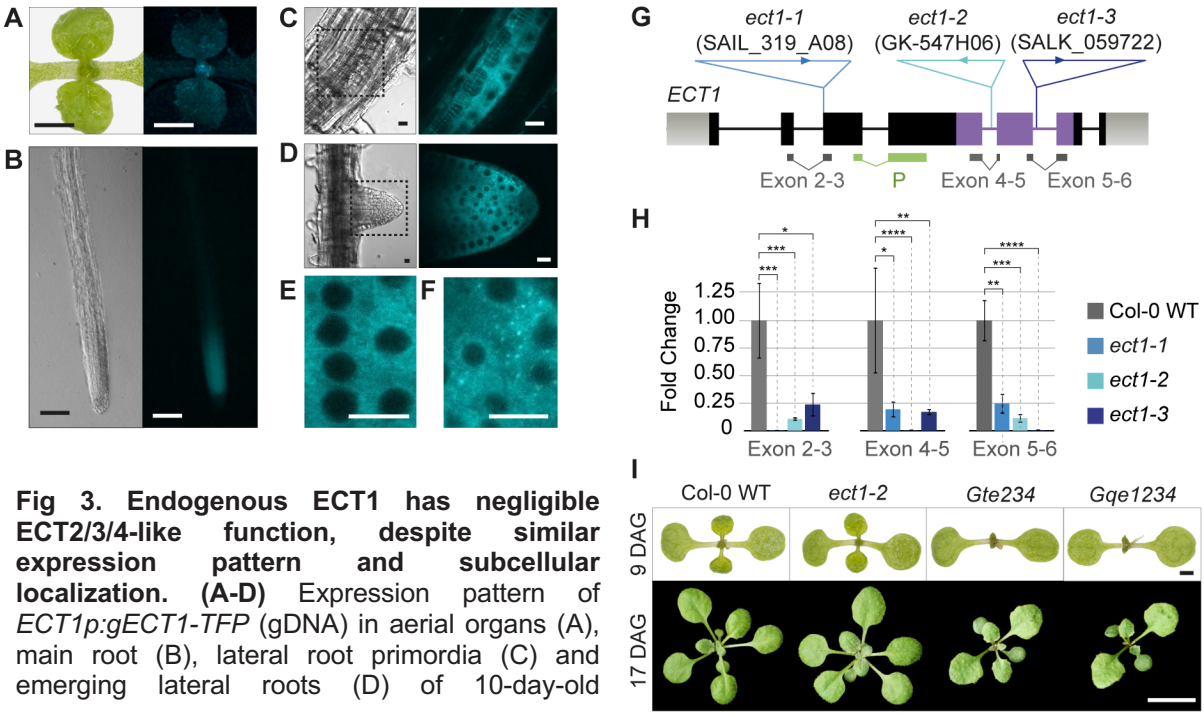

367

368 **Fig 3. Endogenous ECT1 has negligible**
369 **ECT2/3/4-like function, despite similar**
370 **expression pattern and subcellular**
371 **localization. (A-D)** Expression pattern of
372 *ECT1p:gECT1-TFP* (gDNA) in aerial organs (A),
373 main root (B), lateral root primordia (C) and
374 emerging lateral roots (D) of 10-day-old

375 seedlings. The expression mimics the pattern observed for ECT2/3/4 (Arribas-Hernández et al.,
376 2020). **(E-F)** Intracellular localization of ECT1-TFP in meristematic cells of root tips in unchallenged
377 conditions. Although the cytoplasmic signal is largely homogenous I, sporadic foci (F) are frequently
378 observed. S13A Fig shows the integrity of the fluorescently tagged protein in independent transgenic
379 lines assessed by protein blot. **(G)** Schematic representation of the *ECT1* locus. Exons are
380 represented as boxes and introns as lines. The positions and identifiers of the T-DNA insertions
381 assigned to the *ect1-1*, *ect1-2* and *ect1-3* alleles are marked, and the location of qPCR amplicons and
382 hybridization probes (P) for analyses is indicated below. Genotyping of *ect* alleles is shown in S13C-F
383 Fig. **(H)** Expression analysis of *ECT1* mRNA in wild type and T-DNA insertion lines by qPCR.
384 *P<0.01, **P<0.001, ***P<0.0001, and ****P<0.00001 in T-test pairwise comparisons (supporting data
385 in S9 Dataset). Northern blot using the probe (P) marked in G detects *ECT1-TFP* mRNA, but the
386 endogenous *ECT1* transcript is below detection limit (S13B Fig). **(I)** Morphological appearance of
387 seedlings with or without *ECT1* in the different backgrounds indicated. Nomenclature and additional
388 phenotyping of these and alternative allele combinations can be found in S14 Fig. DAG, days after
389 germination. Scale bars are: 1 cm in A, 1 mm in B, 100 µm in C, 10 µm in D-F, 1 mm in upper panels
390 of I, and 1 cm in the lower panels.
391

392 *Mutation of ECT1 does not exacerbate the phenotype of ect2/ect3/ect4 plants*

393 We isolated three homozygous knockout lines caused by T-DNA insertions in the *ECT1*
394 gene, *ect1-1*, *ect1-2*, and *ect1-3* (Figs 3G,H and S13C-F), and crossed two of them to
395 different *ect2/ect3/ect4* triple mutants [16, 17] to obtain two independent allele combinations
396 of quadruple *ect* mutants, *qe1234* and *Gqe1234* (see S14A Fig for nomenclature). In both
397 cases, the quadruple mutant plants were indistinguishable from the corresponding *te234* and
398 *Gte234* triple mutant parentals (Figs 3I and S14B). Similarly, triple *ect1/ect2/ect3* mutants
399 were identical to double *ect2/ect3* mutants, and single *ect1* mutants did not show any
400 obvious defects in *ect2/3*-associated traits such as leaf or root organogenesis and trichome
401 branching (Figs 3I and S14B-D). Thus, despite their similar expression pattern, there is no
402 indication of redundancy between ECT1 and the other three *Ath* DF-A paralogs. This
403 unexpected conclusion agrees with the poor ECT2/3/4-like activity of ECT1 in our functional
404 assay, thereby validating the approach.
405

406 *The divergent function of ECT1 and ECT11 is caused mainly by properties of their IDRs*

407 Having established that different molecular functions are represented in the arabidopsis
408 YTHDF family, we went on to map the molecular regions responsible for this functional
409 divergence. First, we investigated whether lack of *te234* complementation by ECT1/9/11 is
410 due to altered target binding by the YTH domain, IDR-related effector functions, or a
411 combination of both. Thus, we built chimeric IDR/YTH constructs between ECT2 and
412 ECT1/9/11 (Fig 4A). We also tested an ECT8$_{IDR}$/ECT2$_{YTH}$ chimera (C-8/2) to assess whether
413 hybrid constructs can at all be functional, choosing ECT8 as a positive control due to its
414 robust complementation of seedling and adult phenotypes (Fig 2C-D,F). Expression of the
415 constructs in *te234* mutants showed that the C-8/2 chimera was fully functional (Figs 4B and
416 S7B, S15), thus validating the approach. The ECT1- and ECT11-derived hybrids showed
417 that their YTH domains retain m^{6}A-binding ability, because the complementation frequencies

for the C-2/1 and C-2/11 chimeras were not zero (Fig 4B), contrary to an m^{6}A-binding deficient point mutant of *ECT2* [16]. They also proved, however, that both the IDR and the YTH domain of these two proteins only retain a reduced degree of function compared to the equivalent regions in ECT2. In particular, the IDRs of both proteins scored lower than their YTH domains when combined with the other half from ECT2 (Fig 4B), pointing to divergence in the IDR as the main cause for different functionality. In wild type ECT1 and ECT11 proteins, the combination of the two poorly-performing parts is likely the cause of the minute ECT2/3/4-like activity.

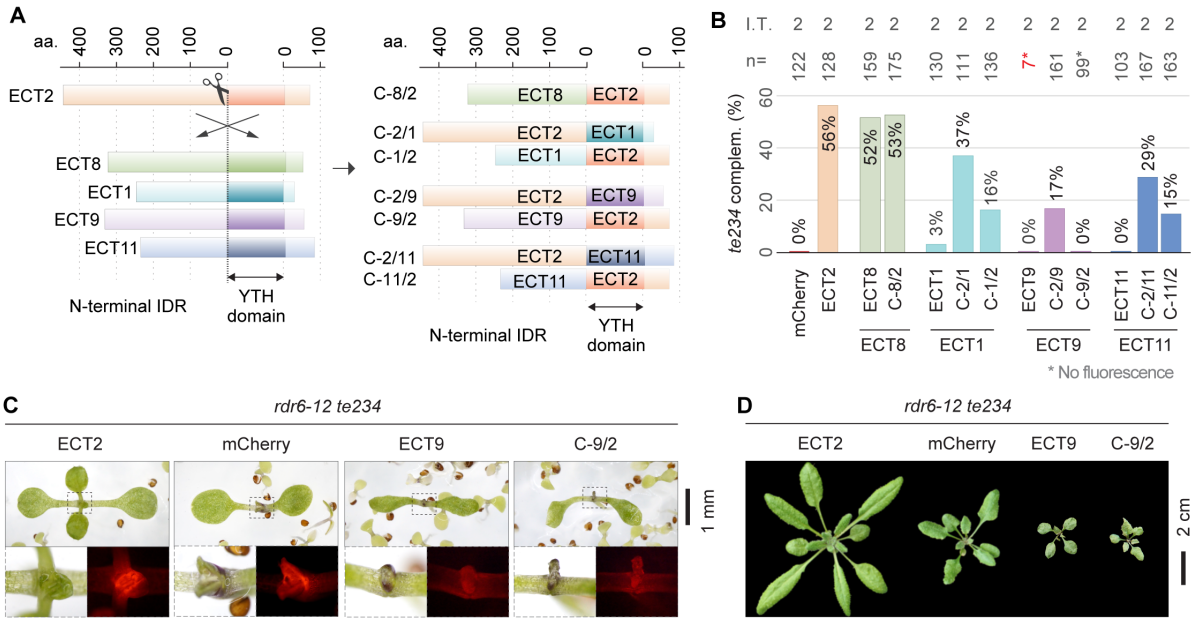

Fig 4. Dissection of ECT1/9/11 functional regions. (A) Schematic representation of the strategy followed to express chimeras with N-terminal IDR and YTH domains of different ECT proteins. **(B)** Weighed averages of the complementation rates observed for each chimeric construct measured as in Fig 2B,C. The raw complementation rates and transformation efficiencies of each independent transformation (I.T.) can be found in Figs S7B and S9 respectively, and photographs of the scored 10-day-old T1 seedlings with mCherry fluorescence are shown in S15 Fig. **(C)** 10-day-old primary transformants of *rdr6-12/te234* with the indicated transgenes. Dashed outlines are magnified below to show mCherry fluorescence. **(D)** Same genotypes as in C at 26 days after germination. Additional independent transgenic lines, developmental stages and controls for C and D can be found in S10 Fig. All transgenes are expressed from the *US7Y* promoter and contain mCherry fused to the C-terminus.

The IDR of ECT9 is incapable of performing ECT2/3/4 molecular functions, but its YTH domain retains some ECT2/3/4-like function

The ECT2$_{IDR}$/ECT9$_{YTH}$ chimera (C-2/9) yielded normal transformation efficiencies and up to 17% of T1s had signs of complementation compared to 56% for ECT2 (Figs 4B and S7B, S9, S15), suggesting that the YTH domain of ECT9 retains at least partial functionality, including m^{6}A-binding activity. However, the reverse construct (ECT9$_{IDR}$/ECT2$_{YTH}$, C-9/2) recapitulated the results obtained for ECT9: low transformation efficiency and low fluorescence in the few T1s recovered, and complete silencing in the next generation (Figs

446 4B and S7B, S9, S15). Hence, we introduced the C-9/2 chimera into the *rdr6-12/te234*
447 background and observed plants with stronger fluorescence exhibiting aberrant morphology,
448 again similar to what was obtained with ECT9 (Figs 4C,D and S7C, S10B). These results
449 confirm that ECT9 is not functionally equivalent to ECT2/3/4, and point to the IDR as the
450 main site of functional divergence of the protein.
451
452 *The molecular requirements for m^{6}A-binding are conserved in the YTH domains of*
453 *ECT1/9/11*
454 To pinpoint molecular characteristics of ECT1/9/11 responsible for their different
455 functionality, we performed a series of comparative analyses between ECT1/9/11 and other
456 ECT proteins. We first analyzed the YTH domains, taking ECT2 as a reference and using
457 the structurally well-characterized YTH domain of *Homo sapiens* (*Hs*) YTHDF1 in complex
458 with RNA GGm^{6}ACU [61] as a model. Amino acid sequence alignment of the YTH domains
459 of all *Ath* ECTs (S16 Fig), AlphaFold-predictions [74, 75] of the apo structures and homology
460 models [76] of the m^{6}A-bound state (S17 Fig) confirmed a high degree of conservation of the
461 key residues required for m^{6}A-RNA binding and overall fold of the YTH domain of
462 ECT1/9/11, in agreement with the partial functionality observed in our chimeric constructs
463 (Fig 4B). However, we also detected a few non-conservative amino acid substitutions
464 specific for ECT1/9/11 (Figs 5A and S16), preferentially located on the surface of the protein
465 but far from the RNA-binding groove (S17 Fig). These non-conservative substitutions are
466 prime candidates to explain the minor differences in functionality, a scenario that implies
467 biological functions of YTH domains other than mere m^{6}A-binding capacity.
468
469 *The IDRs of ECT1/9/11 have biophysical properties distinct from ECT2/3/4/5/6/7/8/10*
470 We next focused on the N-terminal regions of *Ath* ECT1/9/11. Because protein disorder
471 predictions using MobiDB [77] confirmed that they are all disordered (S18 Fig), we used
472 approaches suitable for the study of IDRs. Prediction of short linear motifs (SLiMs) that may
473 mediate interaction with effector proteins gave many possibilities that did not follow a clear
474 pattern when compared between the different ECT classes (S18 Fig). Hence, we decided to
475 study other properties known to be important in IDRs and focused on the propensity to form
476 liquid condensates, the amino acid composition, and the distribution of charge. To determine
477 whether the distinct functional classes of ECTs differed in their propensity to phase
478 separate, we employed a recently developed coarse-grained model of IDRs with residue-
479 specific parameters estimated from experimental observations of many IDRs [78] to simulate
480 their tendency to remain in the condensed phase or disperse in solution. As control, we used
481 the well-studied IDR of the human RNA-binding protein Fused in Sarcoma (FUS) [79-82].
482 The results showed that the IDR of ECT2 has a clear propensity to remain in the condensed

phase (Fig 5B-C and S1 Movie) with a highly favorable Gibb's free energy change for the transition from dilute aqueous solution to condensed phase (Fig 5D), comparable to, albeit not as pronounced as for the IDR of *Hs* FUS (Fig 5B-D). While the IDRs of most *Ath* ECT proteins behaved comparably to ECT2, the IDRs of ECT1 and ECT11 were clear outliers (Figs 5B-D and S19A). Compared to all other ECTs, the IDR of ECT1 showed a much stronger propensity to phase separate, consistent with the spontaneous granule formation of ECT1-TFP *in vivo* (Figs 3F and 5B-D, and S2 Movie). On the contrary, the IDR of ECT11 dispersed into solution much more readily (Fig 5B-D and S3 Movie). Thus, the IDRs of ECT1 and ECT11 have markedly different biophysical properties from those of ECT2/3/4/5/6/7/8/10, perhaps contributing to their different functionality *in vivo*. In contrast, the IDR of ECT9 did not stand out from the rest in the simulations of phase separation propensity. We also note that the different phase separation propensity among the ECTs is driven, in the main, by their different content of sticky residues as defined by the CALVADOS model [78] (S19B Fig). In this context, it is potentially of interest that ECT1, ECT9 and ECT11 all have a higher content of Phe residues than the nearly Phe-depleted IDRs of ECT2/3/4/5/6/7/8/10 (S19C Fig). For ECT1, whose Tyr and Trp enrichment is comparable to that of ECT2/3/4/5/6/7/8/10 (S19C Fig), the additional enrichment of the similarly sticky Phe may contribute to its more pronounced phase separation propensity.

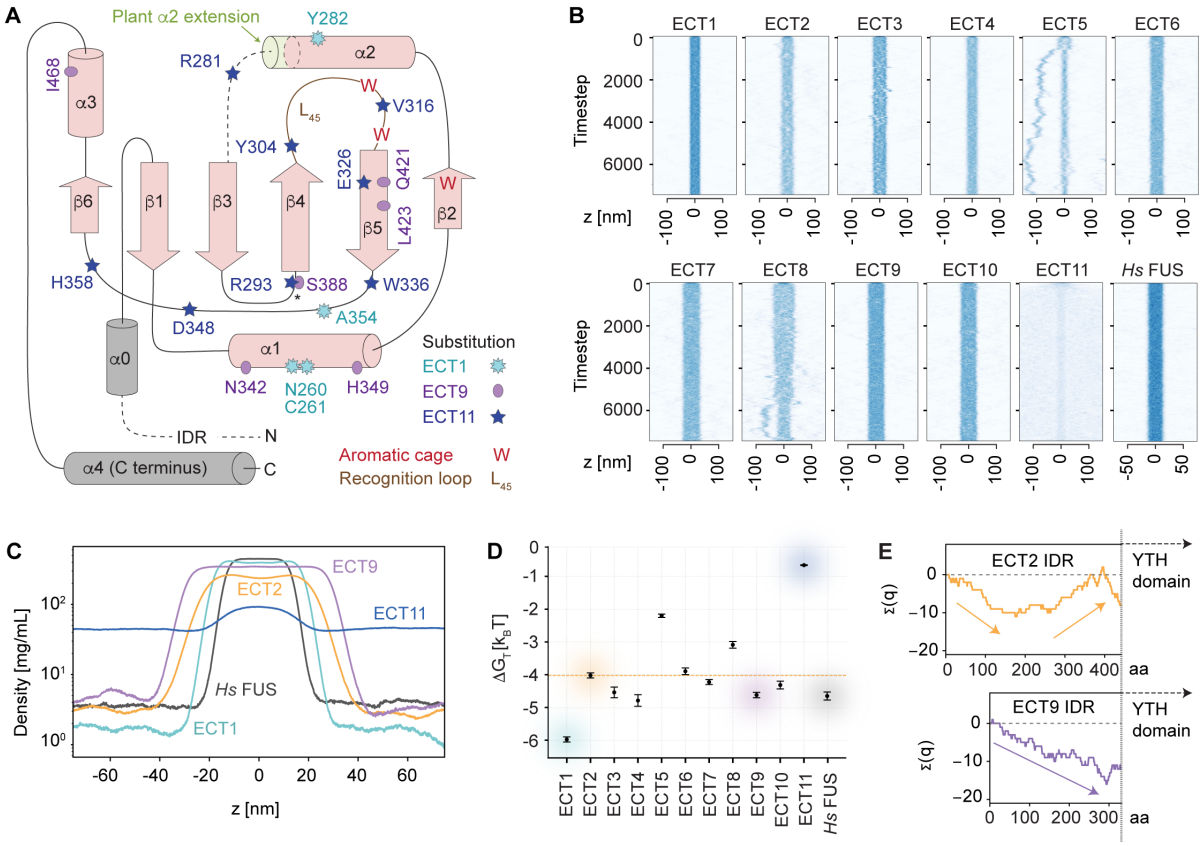

502 **Fig 5. Analysis of ECT1/9/11 functional regions. (A)** Topology of the YTH domain of *Homo sapiens*
503 (*Hs*) YTHDF1 with secondary structure elements drawn in pink [61]. The two grey helices represent
504 the only structural elements outside the YTH domain as defined by Stoilov et al. [8]: α0 immediately
505 upstream, and α4 at the C-terminus of the protein. Superimposed on the diagrams are the non-
506 conservative amino acid substitutions found in *Ath* ECT1, ECT9 and ECT11 compared to the majority
507 of *Ath* ECTs (see alignment in S16 Fig). The localization of these amino acids in the predicted 3D
508 structures, predominantly on the surface, and the spatial integrity of the aromatic cage in the
509 homology models of ECT1/9/11, can be found in S17 Fig. **(B)** Slab simulations of the IDRs of the
510 indicated proteins showing their tendency to remain in condensed phase or disperse in solution.
511 Source videos of ECT2, ECT1 and ECT11 simulations are provided as S1-S3 Movies **(C)** Time-
512 averaged density profiles for a subset of the proteins in B. The analyses of the remaining *Ath* ECTs
513 are shown in S19A Fig. **(D)** Calculated free energy change for the transition between aqueous
514 solution and condensed phase (ΔG_{trans} = RT ln [c_{dilute} / c_{dense}]) for the IDRs of the indicated proteins.
515 **(E)** Cumulative charge distribution of the IDRs of the indicated proteins. The length in amino acids
516 (aa) is at scale. The same analysis for all *Ath* ECTs can be found in S19D Fig.
517

518 We finally analyzed the charge distribution, as this may dictate properties such as
519 compactness and shape of IDR conformations [83, 84]. We found that the IDRs of
520 ECT2/3/4/5/6/7/8/10 show a recurrent pattern with accumulation of net negative charge
521 towards the N-terminus, and recovery to near-neutrality closer to the YTH domain, resulting
522 in creation of electric dipoles (Figs 5E and S19D). The IDRs of ECT1, ECT9 and ECT11
523 differ from this pattern, but in distinct ways: ECT1 does not show a pronounced patterning of
524 the charged residues, while ECT9 increasingly accumulates negative charge (Fig 5E) and
525 ECT11 increasingly accumulates positive charge (S19D Fig). It is an interesting possibility,
526 therefore, that charge separation in the IDR is a requirement to fulfill the molecular functions
527 of ECTs to accelerate growth in primordial cells.
528

529 *The ability to complement ect2/3/4 does not simply follow affiliation with phylogenetic clades*
530 We next compared the functional groups of YTHDF proteins defined by our
531 complementation assays with the YTHDF phylogeny. Strikingly, the ability to rescue
532 defective timing of leaf emergence does not follow the defined phylogenetic clades, because
533 both high and low/null complementation capacities are present in the same clades. For
534 example, ECT2, ECT5 and ECT8 in clades DF-A, -B and -C respectively present high
535 ECT2/3/4-like functionality, while ECT1, ECT9 and ECT11 in these same clades do not (Figs
536 1B and 2C-H). It is noteworthy, however, that there is a clear trend for non-complementors
537 to be amongst the most highly divergent proteins in each group, as revealed by the length of
538 the branches in the phylogenetic tree (Fig 1B). Indeed, some of the longest branches in both
539 our tree and the one in the study by Scutenaire et al. [26] correspond to ECT1, ECT9, and
540 ECT11. Accordingly, the three proteins have the highest number of amino acid substitutions
541 compared to the only YTHDF protein of the liverwort *Marchantia polymorpha* (*Mpo* DFE) [85]
542 (Fig 6A). These results suggest that the common ancestor of YTHDF proteins in land plants

may have had a molecular function related to that of the modern *Ath* ECT2/3/4, and that this function has been conserved in the least-divergent members of the DF-A/B/C/D clades. Subsequent duplication and neofunctionalization may have driven the rapid evolution of highly-divergent YTHDF proteins (ECT11, ECT1, and ECT9 in arabidopsis) that have lost their primary function and perhaps fulfill different molecular roles in the plant m^{6}A pathway.

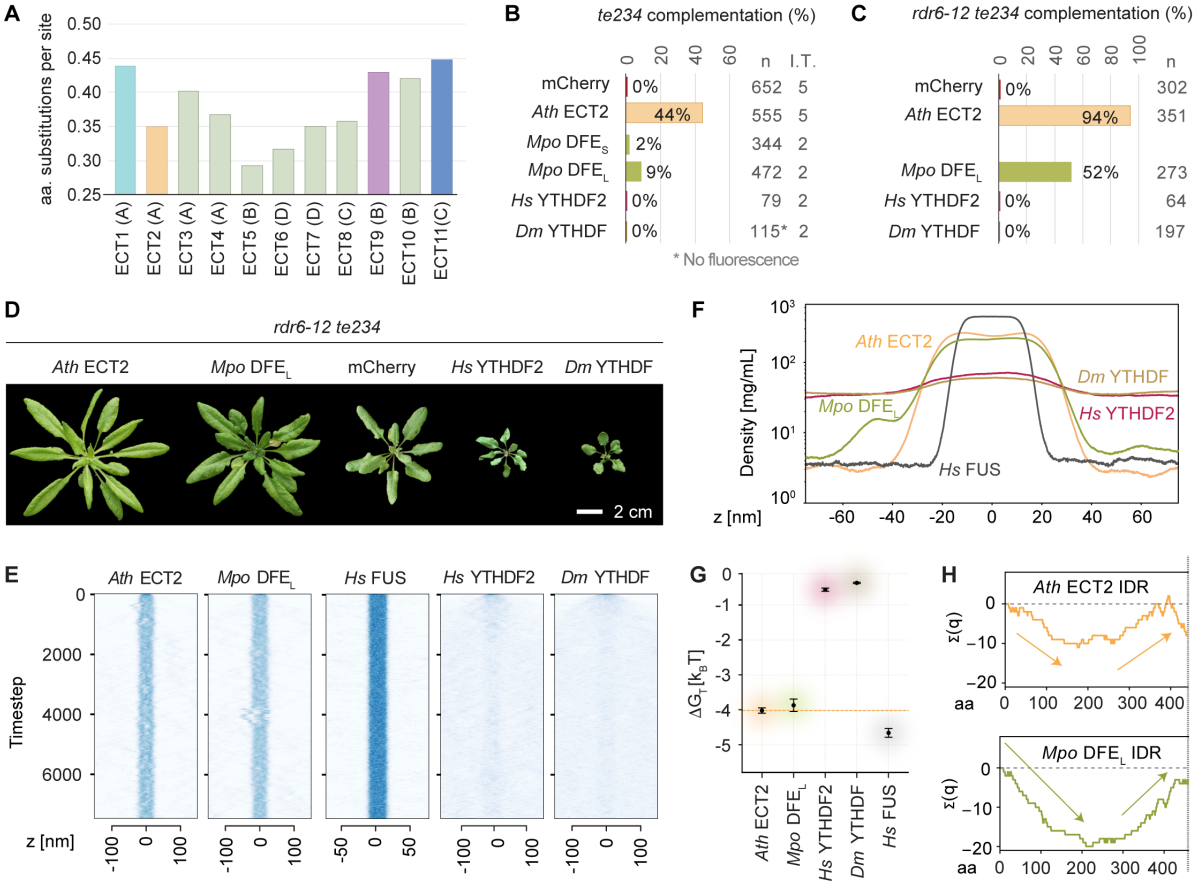

Fig 6. Heterologous expression of a bryophyte DFE rescues loss of ECT2/3/4 function in arabidopsis, while metazoan YTHDF proteins aggravates it. (A) Evolutionary divergence of *Arabidopsis thaliana* (*Ath*) ECT proteins estimated by pairwise comparisons between these and the only DF protein in *Marchantia polymorpha* (*Mpo* DFE) according to the alignment of YTHDFs from bryophytes and angiosperms in S7-S8 Datasets (see Methods). **(B-C)** Weighed averages of the complementation rates observed for *Mpo* DFE (S/L refer to the Short and Long splice forms found in meristematic tissues–apical notches and gemma cups–of *M. polymorpha* thalli), *Homo sapiens* (*Hs*) YTHDF2 and *Drosophila melanogaster* (*Dm*) YTHDF in the *te234* (B) or *rdr6-12/te234* (C) backgrounds, calculated as in Fig 2C-D. n, total number of transformants; I.T. number of independent transformations (only one in C). Raw T1 counts, complementation rates and transformation efficiencies can be found in the S6 Dataset, and S7 and S9 Figs. **(D)** 32-day-old primary transformants expressing the transgenes analysed in C. Additional controls and developmental stages are shown in S10B Fig. **(E)** Slab simulations of the IDRs of the indicated proteins as in Fig 5B. **(F)** Time-averaged density profiles of the slab simulations in E. **(G)** Calculated free energy change for the IDRs of the indicated proteins as in Fig 5D. **(H)** Cumulative charge distribution of the IDRs of the indicated proteins, as in Fig 5E. The same analysis for the two metazoan YTHDFs can be found in S19D Fig.

567 *The molecular function of ECT2/3/4 was present in the first land plants*
568 To test whether the common ancestor of plant YTHDF proteins indeed had a molecular
569 function similar to that of the modern *Ath* ECT2/3/4, we subjected *Mpo* DFE (Fig 2A) to our
570 functional assay, as bryophytes are the earliest-diverging taxon of land plants (Fig 1A, [54,
571 56-60]). The result showed a partial, but clear capacity of two different splice forms of *Mpo*
572 DFE to complement the delay in leaf emergence and morphology defects of arabidopsis
573 *te234* plants (Fig 6B and S7D, S20A-B). Although the complementation scores were low (Fig
574 6B), a thorough inspection of the fluorescence intensity in all primary transformants revealed
575 that the transgene was only expressed very weakly in a reduced subpopulation of plants,
576 possibly due to the tendency to trigger silencing upon heterologous expression of a long
577 cDNA from a distant plant species [86]. We therefore introduced the best-complementing
578 isoform into *rdr6-12/te234* mutants. This approach yielded a much higher complementation
579 score of 52% (Fig 6C), and plants very similar to those expressing ECT2 in the same
580 background (Fig 6D and S6B). Thus, the *Ath* ECT2/3/4 activity needed to stimulate
581 proliferation of primed stem cells was present in the first embryophytes, suggesting that this
582 activity is an ancestral molecular function of YTHDF proteins in land plants. Gratifyingly, the
583 simulations of the behavior of the IDR of *Mpo* DFE showed a dipole-like charge pattern and
584 a phase separation propensity similar to those of the ECT2/3/4/5/6/7/8/10 group, further
585 substantiating that these IDR characteristics correlate with the ability to fulfill ECT2/3/4
586 function in leaf formation (Fig 6E-H). We investigated this interesting possibility more deeply
587 by analysing the IDRs of YTHDF proteins from species representing the main clades of land
588 plants that diverged prior to flower evolution, a moss, a lycophyte, a fern and a gymnosperm,
589 and from the sole species in the sister group to all flowering plants, *A. trichopoda* [87, 88].
590 This analysis showed that at least one YTHDF protein with ECT2-like charge distribution and
591 phase separation propensity is present in all these taxa (S21A Fig). In particular, this
592 included the only YTHDF protein in the moss *Ceratodum purpureus*. Interestingly, when the
593 proteins from the different taxa were analysed together, a general trend for increased phase
594 separation propensity that again correlated with higher 'stickiness' (λ) was apparent in
595 proteins of clades -A, -B and -E compared to those of -C, -D and -F (S21B Fig). We also
596 noticed that in the species that encode multiple YTHDF proteins, some paralogs exhibit
597 divergent IDR features similar to those seen in *Ath* ECT1/9/11, but this phenomenon was not
598 clade-specific (S21 Fig). This result suggests that the IDR-based functional diversification
599 observed in arabidopsis may apply more generally. We conclude that the molecular function
600 of YTHDF proteins required for stimulation of primordial cell proliferation is deeply conserved
601 in land plants, and that the biophysical properties of the IDRs of *Mpo* DFE and the *Ath* DF
602 proteins capable of performing this function are recurrent in all the major plant taxa.
603

604 *Heterologous expression of animal YTHDFs enhances the phenotype caused by loss of*
605 *ECT2/3/4 in Arabidopsis*
606 Finally, we subjected *Hs* YTHDF2 and *Drosophila melanogaster* (*Dm*) YTHDF (Fig 2A) to
607 our functional assay to test whether they could function molecularly like plant YTHDFs.
608 While we did not observe complementation of the delayed leaf emergence of *te234* plants in
609 any of the transformants (Figs 6B and S7D), several *Hs* YTHDF2 lines showed more acute
610 developmental defects compared to *te234* (S20B Fig). Although these defects were not
611 observed among *Dm* YTHDF lines, no expression could be detected in these plants either
612 (S7D Fig). Hence, we repeated the transformation in the *rdr6-12/te234* background, this time
613 obtaining numerous transformants of both *Dm* YTHDF and *Hs* YTHDF2 with strong
614 fluorescence (Figs 6C and S10B). These plants showed aberrant morphology comparable to
615 the effect caused by expression of ECT9 and C-9/2, with resemblance to arabidopsis
616 mutants with severe depletion of m^6A [51, 52] (Figs 6D and S10B). Thus, expression of
617 metazoan YTHDFs in arabidopsis *ECT2/3/4*-deficient plants exacerbates their
618 developmental phenotype. This result is in agreement with the generally accepted idea that
619 m^6A-YTHDF2 destabilizes mRNA in mammals [9, 89-92] while the m^6A/ECT2/3/4 axis does
620 the opposite in plants [23, 51, 93-97]. However, an analogous molecular mechanism
621 between plant and animal YTHDFs cannot be completely ruled out, because a different
622 cellular context may be hampering the molecular activity of metazoan YTHDFs in plant cells,
623 and simple competition for targets with remaining ECTs could be the cause of the enhanced
624 phenotype. Nonetheless, we note that the IDRs of *Hs* YTHDF2 and *Dm* YTHDF had much
625 weaker phase separation propensity (Fig 6E-G) and different charge distribution (S19D Fig)
626 compared to ECT2, perhaps contributing to the lack of ECT2/3-like function *in planta*.
627
628 **Discussion**
629 Our study combines thorough phylogenetic analyses with functional complementation to
630 assess the extent to which molecular functions of YTHDF proteins have diverged over the
631 course of land plant evolution. The key observation is that 8 of the 11 *Ath* ECTs and,
632 remarkably, the sole YTHDF of the liverwort *M. polymorpha*, have the molecular functions
633 required for leaf development in arabidopsis. Along with the refined phylogenetic
634 relationships between plant YTHDFs that we present, these findings have implications for
635 our understanding of three distinct, if obviously related, areas that we discuss in more detail
636 below: (1) the molecular properties of land plant YTHDF proteins, (2) the ancestral YTHDF
637 functions and the evolutionary paths towards YTHDF diversification, and (3) the biology
638 underlying the recurrent employment of expanded YTHDF families in higher plants.
639
640

641 *1. Inferences on molecular properties of land plant YTHDF proteins*
642 Our study provides at least four new insights into molecular properties of land plants YTHDF
643 proteins, all of which are important for future, more detailed mechanistic studies of
644 eukaryotic m^6A-YTHDF function. First, the functional assays with *Ath* ECT proteins and the
645 chimeras combining the YTH domain of ECT1/9/11 with the IDR of ECT2 allow us to infer
646 that all 11 arabidopsis YTHDFs have m^6A-binding capacity, and suggest that some, if not all,
647 of their *in vivo* functions involve m^6A binding. Second, the complementation analyses of the
648 reverse chimeras show that the IDRs of *Ath* ECTs with divergent functions contribute
649 substantially to their different molecular properties. This finding implies a key role of IDRs in
650 defining the molecular activities of YTHDF proteins, and is in line with the conclusions of a
651 recent study of mammalian YTHDFs [48], with the functional importance of the IDR of *Hs*
652 YTHDF2 inferred from early tethering studies [9], and with the isolation of IDR-dependent
653 interactors proposed to be important for *Hs* YTHDF2 and *Ath* ECT2 function [28-30, 96, 98].
654 Third, the ability to direct correct leaf formation correlates with a combination of two
655 biophysical properties of the IDRs of plant YTHDFs: a clear propensity to phase separate,
656 and an organization of charged residues that creates an electric dipole. Future studies are
657 needed to address whether a causal relation underlies this correlation, and, if so, what its
658 molecular basis is. Fourth, amino acid substitutions in YTH domains inferred to be capable
659 of binding to m^6A also contribute, to a lower extent, to functional specialization. Because
660 most affected amino acids are surface-exposed but not predicted to contact RNA, this
661 observation indicates that YTH domains should not be seen as inert adaptors for m^6A
662 association, as they may also participate in effector functions. It is an important goal of future
663 studies to identify such functions and define how they contribute to functional diversification.
664
665 *2. The ancestral function and evolution of YTHDF proteins*
666 It is a key finding of our study that the sole *M. polymorpha* YTHDF protein possesses the
667 molecular functions necessary for leaf formation in flowering plants. This remarkable result
668 demonstrates deep functional conservation, across at least 450 My of evolution, and
669 suggests that stimulating cell division in organ primordia may be the ancestral function of
670 land plant YTHDFs. It is now a question of profound interest to determine how the molecular
671 activity of the ancient YTHDF proteins evolved and diversified as the main eukaryotic linages
672 came into existence. Our work provides several important new insights to guide the
673 understanding of this process. In particular, since it is a valid question whether the main
674 evolutionary event that gave rise to the ancestral function of land plant YTHDFs occurred
675 prior to their terrestrialization, we open this section of the discussion with considerations on
676 how the available information on algal YTHDF proteins informs the debate. We close with

677 the analysis of *Ath* ECT1 divergence as a case study on evolution of specialized YTHDF
678 function.
679
680 *2a. YTHDF proteins in chlorophyte algae are either lost or highly divergent*
681 The genomes of most of the chlorophyte species sequenced thus far do not contain *YTHDF*
682 genes. Indeed, the single YTH domain protein in the model green alga *Chlamydomonas*
683 *reinhardtii* belongs to the DC clade [26, 68], and the same is true for all the species that we
684 inspected in this and five additional orders (S2 Fig). We only found YTHDF-encoding genes
685 in a subset of species in the basal group Mamiellophyceae (S2 Fig). Like land plant,
686 metazoan and yeast YTHDF proteins, these chlorophyte YTHDFs have long N-terminal
687 IDRs and no folded domains other than the YTH domain. Nevertheless, YTHDFs have
688 diverged remarkably fast in Chlorophyta, as revealed by their long branches in the
689 phylogenetic tree, well surpassing that of YTHDF proteins in streptophytes (land plants and
690 charophyte algae) and even the microalgal species of Glaucophyta, Rhizaria and
691 Haptophyta used as outgroup [99, 100] (left bottom corner in Fig 1B, and S1 Fig).
692 Furthermore, the amino acid substitutions and insertions found in some of the proteins affect
693 the aromatic cage (S3 Fig), likely compromising their m^6A-binding capacity. Hence, YTHDF
694 proteins are poorly represented in chlorophytes and, as for the only YTH-domain protein of
695 fission yeast Mmi1 [69], they may have lost m^6A-related functions altogether.
696
697 *2b. YTHDF proteins are widespread and variably divergent in the sister clade of land plants*
698 Another informative group of green algae is the charophytes, or streptophyte algae,
699 photosynthetic organisms that thrive in fresh water or humid terrestrial habitats. Their
700 ancestors split from chlorophytes over a billion years ago and gave rise to all land plants and
701 extant charophytes, [55, 62, 101]. The genomes of most charophyte species sequenced
702 thus far encode YTHDF proteins (Fig S2) with intact aromatic cages and overall higher
703 conservation than those of chlorophytes (Fig S3), but some of them also differ considerably
704 from their closest land plant relatives (Figs 1B and S1, S3), and may include additional
705 folded and even transmembrane domains (S22 Fig).
706
707 *2c. Possible evolutionary scenarios*
708 In the light of the observations regarding YTHDFs in green algae, we consider three possible
709 scenarios for the acquisition of ECT2-like molecular functions in land plants:
710 1) The acquisition occurred during the terrestrialization of the common ancestor of all land
711 plants or, at the latest, within the time window between terrestrialization and bryophyte
712 divergence. In that case, charophyte YTHDFs should not exhibit ECT2-like functionality.

713 2) The acquisition occurred early during streptophyte algae evolution. We consider this the
714 most likely scenario, because such acquisition could have served as exaptation (pre-
715 adaptation) for the successful colonization of dry land, perhaps by contributing to the
716 appearance of apical meristems [55, 102]. The prediction in that case would be that
717 charophytes from late-diverging clades, but not from basal groups, encode YTHDFs with
718 ECT2-like functions.
719 3) The key evolutionary event occurred much earlier, perhaps upon chloroplast acquisition
720 by the last common ancestor of Viridiplantae, Rhodophyta and Glaucophyta, i.e. the first
721 Archaeoplastida, or even before that. We have, however, not been able to find any YTH
722 domain protein in rhodophytes (red algae), and the only glaucophyte sequenced so far [103]
723 contains a single YTHDF (S2 Fig). These observations, together with the scarcity and great
724 divergence of chlorophyte YTHDFs, suggest that if the functional acquisition indeed
725 happened in ancestral Archaeoplastida or earlier, the function and even the proteins
726 altogether were lost in most green and red algae, but kept in the streptophyte lineage that
727 gave rise to land plants. Future functional studies of YTHDFs from Charophyta and
728 Glaucophyta, and taxa close to Archaeoplastida such as Haptophyta, Rhizaria or
729 Stramenopiles (S2 Fig, [99, 100]) will be key for the dissection of the evolutionary origin of
730 the ECT2-like molecular properties required for plant growth [104].
731
732 *2d. ECT1: a newly evolved gene in a Brassicaceae lineage as a case study*
733 In addition to the fundamental question on evolution of the ancestral molecular function of
734 land plant YTHDFs, it is also of interest to consider what characterizes the evolution of late
735 YTHDF specialization. We examine *Ath* ECT1 as a case study in this regard. A thorough
736 look at phylogenetic analyses from Scutenaire *et al.* [26] reveals that *ECT1* is present only in
737 a few species of Brassicaceae such as *A. thaliana* and *Capsella rubella* (*Cru*). *Brassica*
738 *oleracea* in the same family has a clear homolog of *Ath/Cru ECT3* but not of *ECT1*, other
739 dicots encode *ECT3/1* orthologs in a separate cluster, and monocot DF-As arose from an
740 entirely separate branch (S1 Fig, [26]). Therefore, *ECT1* is the product of a recent
741 duplication of the *ECT3/1* gene in a small subgroup of dicots, that diverged more rapidly
742 than any other DF-A clade member in arabidopsis (Fig 1B, [26]). This observation agrees
743 with our overall conclusion that most YTHDFs in early angiosperms possessed *Ath* ECT2-
744 like molecular functions, and only late events resulted in neofunctionalization of specific
745 paralogs. We note that such rapid divergence appears to result primarily from changes in the
746 IDR. We were able to identify two biophysical properties of the IDR of ECT1—its stronger
747 predicted propensity to phase separate and its charge distribution—that are distinct from the
748 ECT2/3/4/5/6/7/8/10 group, but note that additional changes, e.g. in SLiMs mediating
749 interaction with regulatory factors, may also contribute to the different functionality [98].

750 *3. Functional versus biological redundancy and the need for many YTHDFs*

751 Our study reveals that most YTHDF proteins in higher plants can perform, essentially, the
752 same molecular functions that allow ECT2/3/4 to promote cell proliferation in organ
753 primordia and control organogenesis. We anticipate that this molecular function may be
754 used in distinct biological contexts by ECT5/6/7/8/10 due to different expression patterns
755 and response to stimuli, thereby achieving biological specialization. Such variability in
756 expression patterns can be inferred from available RNA-Seq data in the arabidopsis eFP
757 Browser (BAR.toronto.ca) that show, for example, that ECT8 is primarily expressed during
758 senescence-associated processes, perhaps in connection to re-growth after reversible
759 proliferative arrest [105, 106]. Clearly, however, higher plants do not only use many YTHDF-
760 encoding genes to provide the same molecular function(s) in distinct expression domains, as
761 shown by the specialized molecular activity of *Ath* ECT1, ECT11, and most prominently
762 ECT9. Whether these divergent proteins act to counteract the ECT2/3/4-like function by
763 competing for m^6A-containing transcripts, perhaps halting growth upon stress, or whether
764 they perform entirely independent functions in different tissues or cell types, is open for new
765 investigations.

766 An outstanding question not yet resolved by our study is why higher plants seem to
767 need many YTHDF proteins. Indeed, the number of paralogs in vascular plants well
768 surpasses the three YTHDFs present in most vertebrates [6] and the even smaller sets in
769 other eukaryotes (S2 Fig, [8, 68]). The need for many YTHDFs of considerable variability is
770 all the more puzzling given our demonstration here that the majority of them retains the
771 same molecular functions. Robustness is a commonly given explanation for redundancy, but
772 the same argument could apply to YTHDCs, typically encoded by 0-2 genes in most
773 eukaryotes including land plants [8, 68] (S2 Fig), or methyltransferase subunits, for which
774 only single copies have been maintained during evolution [68]. Therefore, the answer should
775 probably be sought elsewhere. It is clear now that the m^6A/YTHDF axis controls cellular
776 proliferation and organ growth in plants [17, 97], and a major difference between land plants
777 and other complex organisms in that regard is the extreme plasticity of plant development.
778 Because growth and stress responses are also tightly intertwined, it is possible that plants
779 use a plethora m^6A-YTHDF growth-stimulators in different organs, responsive to different
780 stresses and developmental cues, to shape plant architecture in response to stimuli. The
781 answer to the paradox may be in the details: plant YTHDFs responsive to different
782 environmental cues may fine-tune growth programs through slightly different performance
783 and target-binding capacity in partly overlapping expression domains, where they are known
784 to compete for targets [23].

785
786

Materials and Methods

Plant material and growth conditions

All the lines used in this study are in the *A. thaliana* Columbia-0 (Col-0) ecotype. The T-DNA insertion lines *rdr6-12* [72], *ect1-1* (SAIL_319_A08), *ect1-2* (GK-547H06), and *ect1-3* (SALK_059722) were obtained from Nottingham Arabidopsis Stock Centre. The mutants *ect2-3*, *ect3-2*, *ect2-3/ect3-2* (*Gde23*), *ect2-3/ect3-2/ect4-2* (*Gte234*) and *ect2-1/ect3-1/ect4-2* (*te234*) used for genetic crosses or as background to produce transgenic lines, and the primers for genotyping the corresponding alleles, have been previously described [16, 17]. The standard growing conditions used are detailed in S1 Appendix.

Phylogenetic analysis

Amino acid sequences of all YTHDF proteins found in 40 species distributed among the main taxa of Viridiplantae were downloaded from UniProt (Apweiler et al., 2004), TAIR (www.arabidopsis.org), Phytozome [107], GinkgoDB [108], FernBase [109] and PhycoCosm [110, 111] (S1 Dataset). As outgroup, we selected three species from the eukaryotic taxa Glaucophyta (*Cyanophora paradoxa, Cpa*), Haptophyta (*Emiliania huxleyi, Ehu*) and Rhizaria (*Paulinella microscpora, Pmi*), as these are evolutionarily closer to Viridiplantae than e.g. Opisthokonta such as animals and fungi [99, 100]. All sequences were aligned with MUSCLE [112, 113] using default parameters (S2 Dataset). The alignment was trimmed from both ends to discard regions with poor sequence conservation according to the quality and conservation scores provided by Jalview [114] (S3 Dataset and S23 Fig). The retained part of the alignment, comparable to the region used for phylogenetic analysis in a previous study [26], contains the entire canonical YTH domain [8] and, on both sides, short stretches with high conservation scores (S23 Fig). Evolutionary analyses were conducted using the maximum likelihood algorithm IQ-Tree 2 [115, 116] from the CIPRES Science Gateway v. 3.3 (https://www.phylo.org/index.php/) to infer a phylogenetic tree. The model based on Q matrix [117] estimated for plants [118], 'Q.plant+R8', was determined as best-fit using the built-in tool ModelFinder [119] according to Bayesian Information Criterion (BIC) scores, and used for the analysis. Measures of branch supports by approximate Likelihood Ratio Test [aLRT] (SH-aLRT, %) [120] were also calculated. The resulting tree (S4 Dataset) was rooted on *Pmi* YTHDF, annotated adding SH-aLRT values, and color-coded using FigTree (https://github.com/rambaut/figtree/). An additional alignment performed with a subset of these proteins with the purpose to illustrate the conservation of the YTH domain in green algae and non-flowering plants was calculated and trimmed as described above (S5 Dataset). The graphical representations of this alignment (S3 and S4 Figs) were obtained using Jalview [114].

823 Estimates of evolutionary divergence between *A. thaliana* and *M. polymorpha*
824 YTHDF proteins were obtained computing pairwise distances from the full length alignment
825 of homologs in a subset of land plant species (bryophytes, basal angiosperms, magnoliids
826 and dicots) (S6 Dataset). These taxa were chosen based on the observation that inclusion of
827 divergent proteins from green algae, ferns, gymnosperms and monocots causes loss of
828 information due to more frequent gaps, while proteins from species closely related to *M.*
829 *polymorpha* (bryophytes) and *A. thaliana* (dicots and basal angiosperms) maximize the
830 accuracy of the alignment. The analysis was done as described above, and we used the
831 Equal Input model [121] in MEGA11 [122] to calculate the distances. All positions containing
832 gaps and missing data were eliminated (complete deletion option), resulting a total of 171
833 positions in the final dataset. The complete matrix as well can be found in S7 Dataset.
834
835 *Cloning, plant transformation and line selection*
836 We employed the scar-free USER cloning method [123] to produce *US7Yp:cYTHDF(X)-*
837 *mCherry-OCSter* and *ECT1p:gECT1-FLAG-TFP-ECT1ter* constructs by gluing PCR-
838 amplified DNA fragments into the pCAMBIA3300-U plasmid [124] that provides resistance to
839 glufosinate in plants. Cloning of the trial *ECT2p:gECT1-mCherry-ECT2ter* and
840 *ECT2p:gECT4-mCherry-ECT2ter* constructs was done with GreenGate [125]. The detailed
841 cloning, transformation and line selection strategy for each construct, as well as the specific
842 details of T1 selections for the complementation assay, are explained in S1 Appendix.
843
844 *IDR modeling and simulations*
845 We carried out coarse-grained simulations of protein IDRs using the implicit-solvent
846 CALVADOS 2 forcefield [78]. In CALVADOS, amino-acid residues are mapped to single
847 beads corresponding to their amino-acid type. Neighboring residues are linked using
848 harmonic bonds with an equilibrium distance of 0.38 nm and force constant of 8033 kJ mol^{-}
849 ^{1}nm^{-2}. Nonbonded interactions are modeled with a hydropathy amino-acid "stickiness" model
850 using λ-parameters from CALVADOS 2 [78, 126]. Salt-screened electrostatic interactions
851 are accounted for with a truncated (r_c = 4 nm) and shifted Debye-Hückel potential; non-
852 electrostatic interactions were truncated at 2 nm [126]. We used a Langevin integrator with
853 friction coefficient γ = 0.01 ps^{-1} to propagate the simulation in 0.01 ps timesteps. All
854 simulations were carried out at T = 293 K.
855 We performed slab simulations of IDRs of the following proteins: *Ath* ECT1-11, *Dm*
856 YTHDF1, *Hs* YTHDF2 and FUS, *Mpo* DFE, *Cpu* DFE, *Ita* DFE1-3, *Cri* DFF1-3, DFAB and
857 DFD1-2, *Gbi* DFF1-2, DFA1-2, DFB, DFC1-2 and DFD, and *Atr* DFA1, DFB, DFC1-2 and
858 DFD, using a previously described procedure [126, 127]. IDR sequences of all proteins are
859 detailed in S1 Dataset. Briefly, we simulated 100 copies of each IDR (one type of IDR at a

860 time) in a simulation slab of dimensions 17x17x300 nm for *Ath* ECT1/3/6-11, *Gbi* DFB and
861 DFF1 and *Atr* DFC2, 15x15x150 nm for *Hs* FUS, or 25x25x300 nm for all other proteins,
862 accounting for the different IDR sequence lengths. We simulated each system for 7500 ns
863 and recorded configurations at 1-ns intervals. The first 2000 ns of each simulation were
864 considered as equilibration and not used for analysis. We centered the protein condensates
865 in the z-dimension of the simulation box during post-processing. The concentrations of the
866 dense phase and dilute phase were calculated by fitting the concentration profiles to a
867 hyperbolic function, as described by Tesei *et al.* [78]. Excess transfer free energies were
868 calculated from the dilute and dense phase equilibrium concentrations via ΔG_{trans} = RT ln
869 (c_{dilute} / c_{dense}) [128]. All simulation data and analysis scripts are available at the Zenodo
870 repository (https://doi.org/10.5281/zenodo.8269719).
871 Charges (q) were added along the IDR sequences to obtain cumulative charge plots.
872 Arg and Lys residues were assigned charges of q = +1; Glu and Asp residues were
873 assigned charges of q = -1; other residue types, including His, were assigned charges of q =
874 0. The average 'stickiness' of a given IDR sequence was determined by calculating the
875 mean hydrophobicity $\bar{\lambda}$ of the IDR amino acid composition, using the CALVADOS 2
876 hydrophobicity scale reported in [126].
877
878 *Additional methods*
879 S1 Appendix describes additional standard methods including DNA and cDNA obtention,
880 genotyping (see S13C-F Fig and S2 Table for additional details), fluorescence microscopy,
881 qPCR (see S9 Dataset for the raw data), RNA and protein blotting, and the characterization
882 of YTH domains.
883
884 **Acknowledgements**
885 We thank Lena Bjørn Johansson, Sergio D'Anna, Jakub Najbar and Tobias Lahti for
886 technical assistance, Theo Bølsterli and his team for plant care, and the Danish National Life
887 Science Supercomputing Center Computerome and the core facility for biocomputing at the
888 Department of Biology (University of Copenhagen) for the use of computational resources.
889 We acknowledge the constructive criticism of Rupert Fray as a reviewer on previous
890 publications, as his suggestion to use the *ect2/ect3/ect4* triple mutant phenotype to test ECT
891 molecular function by systematic ectopic expression in the ECT2 expression domain
892 inspired us to embark on the present project.
893
894 **References**
895
896 1. Zhong S, Li H, Bodi Z, Button J, Vespa L, Herzog M, et al. MTA is an Arabidopsis messenger
897 RNA adenosine methylase and interacts with a homolog of a sex-specific splicing factor. Plant Cell.

898 2008;20(5):1278-88. doi: 10.1105/tpc.108.058883. PubMed PMID: 18505803; PubMed Central
899 PMCID: PMC2438467.

900 2. Geula S, Moshitch-Moshkovitz S, Dominissini D, Mansour AA, Kol N, Salmon-Divon M, et al.
901 m6A mRNA methylation facilitates resolution of naïve pluripotency toward differentiation. Science.
902 2015;347(6225):1002-6. doi: 10.1126/science.1261417.

903 3. Liu N, Dai Q, Zheng G, He C, Parisien M, Pan T. N6-methyladenosine-dependent RNA
904 structural switches regulate RNA-protein interactions. Nature. 2015;518(7540):560-4. doi:
905 10.1038/nature14234. PubMed PMID: 25719671; PubMed Central PMCID: PMC4355918.

906 4. Roost C, Lynch SR, Batista PJ, Qu K, Chang HY, Kool ET. Structure and Thermodynamics of
907 N6-Methyladenosine in RNA: A Spring-Loaded Base Modification. J Am Chem Soc.
908 2015;137(5):2107-15. doi: 10.1021/ja513080v.

909 5. Spitale RC, Flynn RA, Zhang QC, Crisalli P, Lee B, Jung J-W, et al. Structural imprints in vivo
910 decode RNA regulatory mechanisms. Nature. 2015;519(7544):486-90. Epub 2015/03/18. doi:
911 10.1038/nature14263. PubMed PMID: 25799993.

912 6. Patil DP, Pickering BF, Jaffrey SR. Reading m6A in the Transcriptome: m6A-Binding
913 Proteins. Trends Cell Biol. 2018;28(2):113-27. doi: 10.1016/j.tcb.2017.10.001.

914 7. Dominissini D, Moshitch-Moshkovitz S, Schwartz S, Salmon-Divon M, Ungar L, Osenberg S,
915 et al. Topology of the human and mouse m6A RNA methylomes revealed by m6A-seq. Nature.
916 2012;485(7397):201-6. doi: 10.1038/nature11112. PubMed PMID: 22575960.

917 8. Stoilov P, Rafalska I, Stamm S. YTH: a new domain in nuclear proteins. Trends Biochem Sci.
918 2002;27(10):495-7. doi: 10.1016/S0968-0004(02)02189-8.

919 9. Wang X, Lu Z, Gomez A, Hon GC, Yue Y, Han D, et al. N6-methyladenosine-dependent
920 regulation of messenger RNA stability. Nature. 2014;505(7481):117-20. doi: 10.1038/nature12730.
921 PubMed PMID: 24284625.

922 10. Li F, Zhao D, Wu J, Shi Y. Structure of the YTH domain of human YTHDF2 in complex with
923 an m6A mononucleotide reveals an aromatic cage for m6A recognition. Cell Res. 2014;24(12):1490-
924 2. doi: 10.1038/cr.2014.153.

925 11. Luo S, Tong L. Molecular basis for the recognition of methylated adenines in RNA by the
926 eukaryotic YTH domain. Proc Natl Acad Sci USA. 2014;111(38):13834-9. doi:
927 10.1073/pnas.1412742111.

928 12. Theler D, Dominguez C, Blatter M, Boudet J, Allain FH. Solution structure of the YTH domain
929 in complex with N6-methyladenosine RNA: a reader of methylated RNA. Nucleic Acids Res.
930 2014;42(22):13911-9. doi: 10.1093/nar/gku1116. PubMed PMID: 25389274; PubMed Central PMCID:
931 PMC4267619.

932 13. Xu C, Wang X, Liu K, Roundtree IA, Tempel W, Li Y, et al. Structural basis for selective
933 binding of m6A RNA by the YTHDC1 YTH domain. Nat Chem Biol. 2014;10(11):927-9. doi:
934 10.1038/nchembio.1654.

935 14. Zhu T, Roundtree IA, Wang P, Wang X, Wang L, Sun C, et al. Crystal structure of the YTH
936 domain of YTHDF2 reveals mechanism for recognition of N6-methyladenosine. Cell Res.
937 2014;24(12):1493-6. doi: 10.1038/cr.2014.152.

938 15. Zhang Z, Theler D, Kaminska KH, Hiller M, de la Grange P, Pudimat R, et al. The YTH
939 domain is a novel RNA binding domain. The Journal of biological chemistry. 2010;285(19):14701-10.
940 Epub 02/18. doi: 10.1074/jbc.M110.104711. PubMed PMID: 20167602.

941 16. Arribas-Hernández L, Bressendorff S, Hansen MH, Poulsen C, Erdmann S, Brodersen P. An
942 m6A-YTH Module Controls Developmental Timing and Morphogenesis in Arabidopsis. Plant Cell.
943 2018;30(5):952-67.

944 17. Arribas-Hernández L, Simonini S, Hansen MH, Paredes EB, Bressendorff S, Dong Y, et al.
945 Recurrent requirement for the m6A-ECT2/ECT3/ECT4 axis in the control of cell proliferation during
946 plant organogenesis. Development. 2020;147(14):dev189134. doi: 10.1242/dev.189134.

947 18. Lasman L, Krupalnik V, Viukov S, Mor N, Aguilera-Castrejon A, Schneir D, et al. Context-
948 dependent functional compensation between Ythdf m6A reader proteins. Genes Dev. 2020;34(19-
949 20):1373-91.

950 19. Ivanova I, Much C, Di Giacomo M, Azzi C, Morgan M, Moreira PN, et al. The RNA m6A
951 reader YTHDF2 is essential for the post-transcriptional regulation of the maternal transcriptome and
952 oocyte competence. Mol Cell. 2017;67(6):1059-67. doi: 10.1016/j.molcel.2017.08.003.

953 20. Li M, Zhao X, Wang W, Shi H, Pan Q, Lu Z, et al. Ythdf2-mediated m6A mRNA clearance
954 modulates neural development in mice. Genome biology. 2018;19(1):69. doi: 10.1186/s13059-018-
955 1436-y.

956 21. Shi H, Zhang X, Weng Y-L, Lu Z, Liu Y, Lu Z, et al. m6A facilitates hippocampus-dependent
957 learning and memory through YTHDF1. Nature. 2018;563(7730):249-53. doi: 10.1038/s41586-018-
958 0666-1.

959 22. Kontur C, Jeong M, Cifuentes D, Giraldez AJ. Ythdf m6A Readers Function Redundantly
960 during Zebrafish Development. Cell Rep. 2020;33(13):108598. doi: 10.1016/j.celrep.2020.108598.

961 23. Arribas-Hernández L, Rennie S, Schon M, Porcelli C, Enugutti B, Andersson R, et al. The
962 YTHDF proteins ECT2 and ECT3 bind largely overlapping target sets and influence target mRNA
963 abundance, not alternative polyadenylation. eLife. 2021;10:e72377. doi: 10.7554/eLife.72377.

964 24. Lence T, Akhtar J, Bayer M, Schmid K, Spindler L, Ho CH, et al. m6A modulates neuronal
965 functions and sex determination in Drosophila. Nature. 2016;540:242. doi: 10.1038/nature20568.

966 25. Haussmann IU, Bodi Z, Sanchez-Moran E, Mongan NP, Archer N, Fray RG, et al. m6A
967 potentiates Sxl alternative pre-mRNA splicing for robust Drosophila sex determination. Nature.
968 2016;540:301. doi: 10.1038/nature20577.

969 26. Scutenaire J, Deragon J-M, Jean V, Benhamed M, Raynaud C, Favory J-J, et al. The YTH
970 Domain Protein ECT2 Is an m6A Reader Required for Normal Trichome Branching in Arabidopsis.
971 Plant Cell. 2018;30(5):986-1005. doi: 10.1105/tpc.17.00854.

972 27. Li D, Zhang H, Hong Y, Huang L, Li X, Zhang Y, et al. Genome-wide identification,
973 biochemical characterization, and expression analyses of the YTH domain-containing RNA-binding
974 protein family in Arabidopsis and rice. Plant Mol Biol Report. 2014;32(6):1169-86. doi:
975 10.1007/s11105-014-0724-2.

976 28. Du H, Zhao Y, He J, Zhang Y, Xi H, Liu M, et al. YTHDF2 destabilizes m6A-containing RNA
977 through direct recruitment of the CCR4–NOT deadenylase complex. Nat Commun. 2016;7:12626. doi:
978 10.1038/ncomms12626.

979 29. Park OH, Ha H, Lee Y, Boo SH, Kwon DH, Song HK, et al. Endoribonucleolytic Cleavage of
980 m6A-Containing RNAs by RNase P/MRP Complex. Mol Cell. 2019;74(3):494-507.e8. doi:
981 10.1016/j.molcel.2019.02.034.

982 30. Boo SH, Ha H, Lee Y, Shin M-K, Lee S, Kim YK. UPF1 promotes rapid degradation of m6A-
983 containing RNAs. Cell Rep. 2022;39(8):110861. doi: 10.1016/j.celrep.2022.110861.

31. Arribas-Hernández L, Rennie S, Köster T, Porcelli C, Lewinski M, Staiger D, et al. Principles of mRNA targeting via the Arabidopsis m6A-binding protein ECT2. eLife. 2021;10:e72375. doi: 10.7554/eLife.72375.

32. Brodsky S, Jana T, Mittelman K, Chapal M, Kumar DK, Carmi M, et al. Intrinsically Disordered Regions Direct Transcription Factor In Vivo Binding Specificity. Mol Cell. 2020;79(3):459-71.e4. doi: 10.1016/j.molcel.2020.05.032.

33. Wang J, Wang L, Diao J, Shi YG, Shi Y, Ma H, et al. Binding to m6A RNA promotes YTHDF2-mediated phase separation. Protein & Cell. 2020;11(4):304-7. doi: 10.1007/s13238-019-00660-2.

34. Gao Y, Pei G, Li D, Li R, Shao Y, Zhang QC, et al. Multivalent m6A motifs promote phase separation of YTHDF proteins. Cell Res. 2019;29(9):767-9. doi: 10.1038/s41422-019-0210-3.

35. Ries RJ, Zaccara S, Klein P, Olarerin-George A, Namkoong S, Pickering BF, et al. m6A enhances the phase separation potential of mRNA. Nature. 2019;571(7765):424-8. doi: 10.1038/s41586-019-1374-1.

36. Fu Y, Zhuang X. m6A-binding YTHDF proteins promote stress granule formation. Nat Chem Biol. 2020;16(9):955-63. doi: 10.1038/s41589-020-0524-y.

37. Scutenaire J, Plassard D, Matelot M, Villa T, Zumsteg J, Libri D, et al. The S. cerevisiae m6A-reader Pho92 promotes timely meiotic recombination by controlling key methylated transcripts. Nucleic Acids Res. 2022:gkac640. doi: 10.1093/nar/gkac640.

38. Varier RA, Sideri T, Capitanchik C, Manova Z, Calvani E, Rossi A, et al. N6-methyladenosine (m6A) reader Pho92 is recruited co-transcriptionally and couples translation to mRNA decay to promote meiotic fitness in yeast. eLife. 2022;11:e84034. doi: 10.7554/eLife.84034.

39. Zaccara S, Jaffrey SR. A Unified Model for the Function of YTHDF Proteins in Regulating m(6)A-Modified mRNA. Cell. 2020;181(7):1582-95.e18. Epub 2020/06/04. doi: 10.1016/j.cell.2020.05.012. PubMed PMID: 32492408.

40. Ok SH, Jeong HJ, Bae JM, Shin JS, Luan S, Kim KN. Novel CIPK1-associated proteins in Arabidopsis contain an evolutionarily conserved C-terminal region that mediates nuclear localization. Plant Physiol. 2005;139(1):138-50. doi: 10.1104/pp.105.065649. PubMed PMID: 16113215.

41. Bergeron-Sandoval L-P, Safaee N, Michnick Stephen W. Mechanisms and Consequences of Macromolecular Phase Separation. Cell. 2016;165(5):1067-79. doi: 10.1016/j.cell.2016.05.026.

42. Borcherds W, Bremer A, Borgia MB, Mittag T. How do intrinsically disordered protein regions encode a driving force for liquid–liquid phase separation? Curr Opin Struct Biol. 2021;67:41-50. doi: 10.1016/j.sbi.2020.09.004.

43. Murakami S, Jaffrey SR. Hidden codes in mRNA: Control of gene expression by m6A. Mol Cell. 2022;82(12):2236-51. doi: 10.1016/j.molcel.2022.05.029.

44. Wang X, Zhao Boxuan S, Roundtree Ian A, Lu Z, Han D, Ma H, et al. N6-methyladenosine modulates messenger RNA translation efficiency. Cell. 2015;161(6):1388-99. doi: 10.1016/j.cell.2015.05.014.

45. Shi H, Wang X, Lu Z, Zhao BS, Ma H, Hsu PJ, et al. YTHDF3 facilitates translation and decay of N6-methyladenosine-modified RNA. Cell Res. 2017;27:315-28. doi: 10.1038/cr.2017.15.

46. Li A, Chen Y-S, Ping X-L, Yang X, Xiao W, Yang Y, et al. Cytoplasmic m6A reader YTHDF3 promotes mRNA translation. Cell Res. 2017;27:444. doi: 10.1038/cr.2017.10.

1026 47. Li Y, Bedi RK, Moroz-Omori EV, Caflisch A. Structural and Dynamic Insights into Redundant
1027 Function of YTHDF Proteins. Journal of Chemical Information and Modeling. 2020;60(12):5932-5. doi:
1028 10.1021/acs.jcim.0c01029.

1029 48. Zou Z, Sepich-Poore C, Zhou X, Wei J, He C. The mechanism underlying redundant
1030 functions of the YTHDF proteins. Genome biology. 2023;24(1):17. doi: 10.1186/s13059-023-02862-8.

1031 49. Fray RG, Simpson GG. The Arabidopsis epitranscriptome. Curr Opin Plant Biol. 2015;27:17-
1032 21. doi: 10.1016/j.pbi.2015.05.015.

1033 50. Bodi Z, Zhong S, Mehra S, Song J, Graham N, Li H, et al. Adenosine methylation in
1034 Arabidopsis mRNA is associated with the 3' end and reduced levels cause developmental defects.
1035 Front Plant Sci. 2012;3:48. doi: 10.3389/fpls.2012.00048. PubMed PMID: 22639649.

1036 51. Shen L, Liang Z, Gu X, Chen Y, Teo Zhi Wei N, Hou X, et al. N6-methyladenosine RNA
1037 modification regulates shoot stem cell fate in Arabidopsis. Dev Cell. 2016;38(2):186-200. doi:
1038 10.1016/j.devcel.2016.06.008.

1039 52. Růžička K, Zhang M, Campilho A, Bodi Z, Kashif M, Saleh M, et al. Identification of factors
1040 required for m6A mRNA methylation in Arabidopsis reveals a role for the conserved E3 ubiquitin
1041 ligase HAKAI. New Phytol. 2017;215(1):157-72. doi: 10.1111/nph.14586.

1042 53. Pires ND, Dolan L. Morphological evolution in land plants: new designs with old genes.
1043 Philosophical Transactions of the Royal Society B: Biological Sciences. 2012;367(1588):508-18. doi:
1044 10.1098/rstb.2011.0252.

1045 54. One Thousand Plant Transcriptomes I. One thousand plant transcriptomes and
1046 the phylogenomics of green plants. Nature. 2019;574(7780):679-85. Epub 2019/10/23. doi:
1047 10.1038/s41586-019-1693-2. PubMed PMID: 31645766.

1048 55. de Vries J, Archibald JM. Plant evolution: landmarks on the path to terrestrial life. New Phytol.
1049 2018;217(4):1428-34. doi: 10.1111/nph.14975.

1050 56. Harris BJ, Harrison CJ, Hetherington AM, Williams TA. Phylogenomic Evidence for the
1051 Monophyly of Bryophytes and the Reductive Evolution of Stomata. Current Biology.
1052 2020;30(11):2001-12.e2. doi: 10.1016/j.cub.2020.03.048.

1053 57. Li F-W, Nishiyama T, Waller M, Frangedakis E, Keller J, Li Z, et al. Anthoceros genomes
1054 illuminate the origin of land plants and the unique biology of hornworts. Nature plants. 2020;6(3):259-
1055 72. Epub 2020/03/13. doi: 10.1038/s41477-020-0618-2. PubMed PMID: 32170292.

1056 58. Puttick MN, Morris JL, Williams TA, Cox CJ, Edwards D, Kenrick P, et al. The
1057 Interrelationships of Land Plants and the Nature of the Ancestral Embryophyte. Current Biology.
1058 2018;28(5):733-45.e2. doi: 10.1016/j.cub.2018.01.063.

1059 59. Su D, Yang L, Shi X, Ma X, Zhou X, Hedges SB, et al. Large-Scale Phylogenomic Analyses
1060 Reveal the Monophyly of Bryophytes and Neoproterozoic Origin of Land Plants. Mol Biol Evol.
1061 2021;38(8):3332-44. doi: 10.1093/molbev/msab106. PubMed PMID: 33871608.

1062 60. Zhang J, Fu X-X, Li R-Q, Zhao X, Liu Y, Li M-H, et al. The hornwort genome and early land
1063 plant evolution. Nature plants. 2020;6(2):107-18. Epub 2020/02/10. doi: 10.1038/s41477-019-0588-4.
1064 PubMed PMID: 32042158.

1065 61. Xu C, Liu K, Ahmed H, Loppnau P, Schapira M, Min J. Structural Basis for the Discriminative
1066 Recognition of N6-Methyladenosine RNA by the Human YT521-B Homology Domain Family of
1067 Proteins. Journal of Biological Chemistry. 2015;290(41):24902-13. doi: 10.1074/jbc.M115.680389.

1068 62. Bowman JL. The origin of a land flora. Nature Plants. 2022;8(12):1352-69. doi:
1069 10.1038/s41477-022-01283-y.

1070 63. Magallón S, Hilu KW, Quandt D. Land plant evolutionary timeline: Gene effects are secondary
1071 to fossil constraints in relaxed clock estimation of age and substitution rates. Am J Bot.
1072 2013;100(3):556-73. doi: 10.3732/ajb.1200416.

1073 64. Lan T, Xiong W, Chen X, Mo B, Tang G. Plant cytoplasmic ribosomal proteins: an update on
1074 classification, nomenclature, evolution and resources. Plant J. 2022;110(1):292-318. doi:
1075 10.1111/tpj.15667.

1076 65. Scarpin MR, Busche M, Martinez RE, Harper LC, Reiser L, Szakonyi D, et al. An updated
1077 nomenclature for plant ribosomal protein genes. Plant Cell. 2023;35(2):640-3. doi:
1078 10.1093/plcell/koac333.

1079 66. Weijers D, Franke-van Dijk M, Vencken R-J, Quint A, Hooykaas P, Offringa R. An
1080 Arabidopsis Minute-like phenotype caused by a semi-dominant mutation in a RIBOSOMAL PROTEIN
1081 S5 gene. Development. 2001;128(21):4289-99. doi: 10.1242/dev.128.21.4289.

1082 67. Fagard M, Vaucheret H. (TRANS)GENE SILENCING IN PLANTS: How Many Mechanisms?
1083 Annu Rev Plant Physiol Plant Mol Biol. 2000;51(1):167-94. doi: 10.1146/annurev.arplant.51.1.167.

1084 68. Balacco DL, Soller M. The m6A Writer: Rise of a Machine for Growing Tasks. Biochemistry.
1085 2019;58(5):363-78. doi: 10.1021/acs.biochem.8b01166.

1086 69. Wang C, Zhu Y, Bao H, Jiang Y, Xu C, Wu J, et al. A novel RNA-binding mode of the YTH
1087 domain reveals the mechanism for recognition of determinant of selective removal by Mmi1. Nucleic
1088 Acids Res. 2016;44(2):969-82. doi: 10.1093/nar/gkv1382.

1089 70. Dalmay T, Hamilton A, Rudd S, Angell S, Baulcombe DC. An RNA-dependent RNA
1090 polymerase gene in Arabidopsis is required for posttranscriptional gene silencing mediated by a
1091 transgene but not by a virus. Cell. 2000;101(5):543-53. PubMed PMID: 10850496.

1092 71. Mourrain P, Beclin C, Elmayan T, Feuerbach F, Godon C, Morel J-B, et al. *Arabidopsis SGS2*
1093 and *SGS3* genes are required for posttranscriptional gene silencing and natural virus resistance. Cell.
1094 2000;101:533-42.

1095 72. Peragine A, Yoshikawa M, Wu G, Albrecht HL, Poethig RS. SGS3 and SGS2/SDE1/RDR6
1096 are required for juvenile development and the production of trans-acting siRNAs in Arabidopsis.
1097 Genes Dev. 2004;18(19):2368-79. PubMed PMID: 15466488.

1098 73. Zhang H, Zhang F, Yu Y, Feng L, Jia J, Liu B, et al. A Comprehensive Online Database for
1099 Exploring ~20,000 Public Arabidopsis RNA-Seq Libraries. Molecular Plant. 2020;13(9):1231-3. doi:
1100 10.1016/j.molp.2020.08.001.

1101 74. Jumper J, Evans R, Pritzel A, Green T, Figurnov M, Ronneberger O, et al. Highly accurate
1102 protein structure prediction with AlphaFold. Nature. 2021;596(7873):583-9. doi: 10.1038/s41586-021-
1103 03819-2.

1104 75. Varadi M, Anyango S, Deshpande M, Nair S, Natassia C, Yordanova G, et al. AlphaFold
1105 Protein Structure Database: massively expanding the structural coverage of protein-sequence space
1106 with high-accuracy models. Nucleic Acids Res. 2022;50(D1):D439-D44. doi: 10.1093/nar/gkab1061.

1107 76. Biasini M, Bienert S, Waterhouse A, Arnold K, Studer G, Schmidt T, et al. SWISS-MODEL:
1108 modelling protein tertiary and quaternary structure using evolutionary information. Nucleic Acids Res.
1109 2014;42(W1):W252-W8. doi: 10.1093/nar/gku340.

1110 77. Piovesan D, Del Conte A, Clementel D, Monzon Alexander M, Bevilacqua M, Aspromonte
1111 Maria C, et al. MobiDB: 10 years of intrinsically disordered proteins. Nucleic Acids Res.
1112 2023;51(D1):D438-D44. doi: 10.1093/nar/gkac1065.

1113 78. Tesei G, Schulze TK, Crehuet R, Lindorff-Larsen K. Accurate model of liquid-liquid phase
1114 behavior of intrinsically disordered proteins from optimization of single-chain properties. Proc Natl
1115 Acad Sci USA. 2021;118(44):e2111696118. doi: 10.1073/pnas.2111696118. PubMed PMID:
1116 34716273.

1117 79. Kato M, McKnight SL. The low-complexity domain of the FUS RNA binding protein self-
1118 assembles via the mutually exclusive use of two distinct cross-β cores. Proc Natl Acad Sci USA.
1119 2021;118(42):e2114412118. doi: 10.1073/pnas.2114412118.

1120 80. Kato M, Han TW, Xie S, Shi K, Du X, Wu LC, et al. Cell-free formation of RNA granules: low
1121 complexity sequence domains form dynamic fibers within hydrogels. Cell. 2012;149(4):753-67. doi:
1122 10.1016/j.cell.2012.04.017. PubMed PMID: 22579281.

1123 81. Patel A, Lee Hyun O, Jawerth L, Maharana S, Jahnel M, Hein Marco Y, et al. A Liquid-to-
1124 Solid Phase Transition of the ALS Protein FUS Accelerated by Disease Mutation. Cell.
1125 2015;162(5):1066-77. doi: 10.1016/j.cell.2015.07.047.

1126 82. Schwartz Jacob C, Wang X, Podell Elaine R, Cech Thomas R. RNA Seeds Higher-Order
1127 Assembly of FUS Protein. Cell Rep. 2013;5(4):918-25. doi: 10.1016/j.celrep.2013.11.017.

1128 83. Bianchi G, Mangiagalli M, Barbiroli A, Longhi S, Grandori R, Santambrogio C, et al.
1129 Distribution of Charged Residues Affects the Average Size and Shape of Intrinsically Disordered
1130 Proteins. Biomolecules. 2022;12(4). doi: 10.3390/biom12040561.

1131 84. Das RK, Huang Y, Phillips AH, Kriwacki RW, Pappu RV. Cryptic sequence features within the
1132 disordered protein p27Kip1 regulate cell cycle signaling. Proc Natl Acad Sci USA. 2016;113(20):5616-
1133 21. doi: 10.1073/pnas.1516277113.

1134 85. Bowman JL, Kohchi T, Yamato KT, Jenkins J, Shu S, Ishizaki K, et al. Insights into Land
1135 Plant Evolution Garnered from the Marchantia polymorpha Genome. Cell. 2017;171(2):287-304.e15.
1136 doi: 10.1016/j.cell.2017.09.030.

1137 86. Wang L, Roossinck MJ. Comparative analysis of expressed sequences reveals a conserved
1138 pattern of optimal codon usage in plants. Plant Mol Biol. 2006;61(4):699-710. doi: 10.1007/s11103-
1139 006-0041-8.

1140 87. Soltis PS, Soltis DE, Chase MW. Angiosperm phylogeny inferred from multiple genes as a
1141 tool for comparative biology. Nature. 1999;402(6760):402-4. doi: 10.1038/46528.

1142 88. Qiu Y-L, Lee J, Bernasconi-Quadroni F, Soltis DE, Soltis PS, Zanis M, et al. The earliest
1143 angiosperms: evidence from mitochondrial, plastid and nuclear genomes. Nature.
1144 1999;402(6760):404-7. doi: 10.1038/46536.

1145 89. Sommer S, Lavi U, Darnell JE. The absolute frequency of labeled N-6-methyladenosine in
1146 HeLa cell messenger RNA decreases with label time. Journal of Molecular Biology. 1978;124(3):487-
1147 99. doi: 10.1016/0022-2836(78)90183-3.

1148 90. Wang Y, Li Y, Toth JI, Petroski MD, Zhang Z, Zhao JC. N6-methyladenosine modification
1149 destabilizes developmental regulators in embryonic stem cells. Nature cell biology. 2014;16(2):191-8.
1150 doi: 10.1038/ncb2902. PubMed PMID: 24394384.

1151 91. Ke S, Pandya-Jones A, Saito Y, Fak JJ, Vågbø CB, Geula S, et al. m6A mRNA modifications
1152 are deposited in nascent pre-mRNA and are not required for splicing but do specify cytoplasmic
1153 turnover. Genes Dev. 2017;31(10):990-1006.

1154 92. Herzog VA, Reichholf B, Neumann T, Rescheneder P, Bhat P, Burkard TR, et al. Thiol-linked
1155 alkylation of RNA to assess expression dynamics. Nat Meth. 2017;14:1198. doi: 10.1038/nmeth.4435.

1156 93. Anderson SJ, Kramer MC, Gosai SJ, Yu X, Vandivier LE, Nelson ADL, et al. N(6)-
1157 Methyladenosine Inhibits Local Ribonucleolytic Cleavage to Stabilize mRNAs in Arabidopsis. Cell
1158 Rep. 2018;25(5):1146-57. doi: 10.1016/j.celrep.2018.10.020. PubMed PMID: 30380407.

1159 94. Wei L-H, Song P, Wang Y, Lu Z, Tang Q, Yu Q, et al. The m6A Reader ECT2 Controls
1160 Trichome Morphology by Affecting mRNA Stability in Arabidopsis. Plant Cell. 2018;30(5):968-85. doi:
1161 10.1105/tpc.17.00934.

1162 95. Parker MT, Knop K, Sherwood AV, Schurch NJ, Mackinnon K, Gould PD, et al. Nanopore
1163 direct RNA sequencing maps the complexity of Arabidopsis mRNA processing and m6A modification.
1164 eLife. 2020;9:e49658. doi: 10.7554/eLife.49658.

1165 96. Song P, Wei L, Chen Z, Cai Z, Lu Q, Wang C, et al. m6A readers ECT2/ECT3/ECT4 enhance
1166 mRNA stability through direct recruitment of the poly(A) binding proteins in Arabidopsis. Genome
1167 biology. 2023;24(1):103. doi: 10.1186/s13059-023-02947-4.

1168 97. Arribas-Hernández L, Brodersen P. Occurrence and functions of m6A and other covalent
1169 modifications in plant mRNA. Plant Physiol. 2020;182(1):79-96. doi: 10.1104/pp.19.01156.

1170 98. Tankmar MD, Reichel M, Arribas-Hernández L, Brodersen P. A YTHDF-PABP axis is
1171 required for m6A-mediated organogenesis in plants. bioRxiv. 2023:2023.07.03.547513. doi:
1172 10.1101/2023.07.03.547513.

1173 99. Al Jewari C, Baldauf SL. An excavate root for the eukaryote tree of life. Science Advances.
1174 9(17):eade4973. doi: 10.1126/sciadv.ade4973.

1175 100. Burki F, Roger AJ, Brown MW, Simpson AGB. The New Tree of Eukaryotes. Trends in
1176 Ecology & Evolution. 2020;35(1):43-55. doi: 10.1016/j.tree.2019.08.008.

1177 101. McCourt RM, Lewis LA, Strother PK, Delwiche CF, Wickett NJ, de Vries J, et al. Green land:
1178 Multiple perspectives on green algal evolution and the earliest land plants. Am J Bot.
1179 2023;110(5):e16175. doi: 10.1002/ajb2.16175.

1180 102. Graham LE, Cook ME, Busse JS. The origin of plants: Body plan changes contributing to a
1181 major evolutionary radiation. Proc Natl Acad Sci USA. 2000;97(9):4535-40. doi:
1182 10.1073/pnas.97.9.4535.

1183 103. Price DC, Goodenough UW, Roth R, Lee J-H, Kariyawasam T, Mutwil M, et al. Analysis of an
1184 improved Cyanophora paradoxa genome assembly. DNA Research. 2019;26(4):287-99. doi:
1185 10.1093/dnares/dsz009.

1186 104. Van Etten J, Benites LF, Stephens TG, Yoon HS, Bhattacharya D. Algae obscura: The
1187 potential of rare species as model systems. J Phycol. 2023;59(2):293-300. doi: 10.1111/jpy.13321.

1188 105. Gan S. Mitotic and Postmitotic Senescence in Plants. Science of Aging Knowledge
1189 Environment. 2003;2003(38):re7-re. doi: 10.1126/sageke.2003.38.re7.

1190 106. Wuest SE, Philipp MA, Guthörl D, Schmid B, Grossniklaus U. Seed Production Affects
1191 Maternal Growth and Senescence in Arabidopsis Plant Physiol. 2016;171(1):392-404. doi:
1192 10.1104/pp.15.01995.

1193 107. Goodstein DM, Shu S, Howson R, Neupane R, Hayes RD, Fazo J, et al. Phytozome: a
1194 comparative platform for green plant genomics. Nucleic Acids Res. 2012;40(D1):D1178-D86. doi:
1195 10.1093/nar/gkr944.

1196 108. Gu K-J, Lin C-F, Wu J-J, Zhao Y-P. GinkgoDB: an ecological genome database for the living
1197 fossil, Ginkgo biloba. Database. 2022;2022:baac046. doi: 10.1093/database/baac046.

1198 109. Li F-W, Brouwer P, Carretero-Paulet L, Cheng S, de Vries J, Delaux P-M, et al. Fern
1199 genomes elucidate land plant evolution and cyanobacterial symbioses. Nature Plants. 2018;4(7):460-
1200 72. doi: 10.1038/s41477-018-0188-8.

1201 110. Grigoriev IV, Nordberg H, Shabalov I, Aerts A, Cantor M, Goodstein D, et al. The Genome
1202 Portal of the Department of Energy Joint Genome Institute. Nucleic Acids Res. 2012;40(D1):D26-D32.
1203 doi: 10.1093/nar/gkr947.

1204 111. Nordberg H, Cantor M, Dusheyko S, Hua S, Poliakov A, Shabalov I, et al. The genome portal
1205 of the Department of Energy Joint Genome Institute: 2014 updates. Nucleic Acids Res.
1206 2014;42(D1):D26-D31. doi: 10.1093/nar/gkt1069.

1207 112. Edgar RC. MUSCLE: multiple sequence alignment with high accuracy and high throughput.
1208 Nucleic Acids Res. 2004;32(5):1792-7. doi: 10.1093/nar/gkh340. PubMed PMID: 15034147.

1209 113. Edgar RC. MUSCLE: a multiple sequence alignment method with reduced time and space
1210 complexity. BMC Bioinformatics. 2004;5(1):113. doi: 10.1186/1471-2105-5-113.

1211 114. Waterhouse AM, Procter JB, Martin DMA, Clamp M, Barton GJ. Jalview Version 2—a multiple
1212 sequence alignment editor and analysis workbench. Bioinformatics. 2009;25(9):1189-91. doi:
1213 10.1093/bioinformatics/btp033.

1214 115. Nguyen L-T, Schmidt HA, von Haeseler A, Minh BQ. IQ-TREE: A Fast and Effective
1215 Stochastic Algorithm for Estimating Maximum-Likelihood Phylogenies. Mol Biol Evol. 2015;32(1):268-
1216 74. doi: 10.1093/molbev/msu300.

1217 116. Minh BQ, Schmidt HA, Chernomor O, Schrempf D, Woodhams MD, von Haeseler A, et al. IQ-
1218 TREE 2: New Models and Efficient Methods for Phylogenetic Inference in the Genomic Era. Mol Biol
1219 Evol. 2020;37(5):1530-4. doi: 10.1093/molbev/msaa015.

1220 117. Minh BQ, Dang CC, Vinh LS, Lanfear R. QMaker: Fast and Accurate Method to Estimate
1221 Empirical Models of Protein Evolution. Syst Biol. 2021;70(5):1046-60. doi: 10.1093/sysbio/syab010.

1222 118. Ran J-H, Shen T-T, Wang M-M, Wang X-Q. Phylogenomics resolves the deep phylogeny of
1223 seed plants and indicates partial convergent or homoplastic evolution between Gnetales and
1224 angiosperms. Proceedings of the Royal Society B: Biological Sciences. 2018;285(1881):20181012.
1225 doi: 10.1098/rspb.2018.1012.

1226 119. Kalyaanamoorthy S, Minh BQ, Wong TKF, von Haeseler A, Jermiin LS. ModelFinder: fast
1227 model selection for accurate phylogenetic estimates. Nat Meth. 2017;14(6):587-9. Epub 2017/05/08.
1228 doi: 10.1038/nmeth.4285. PubMed PMID: 28481363.

1229 120. Shimodaira H, Hasegawa M. Multiple Comparisons of Log-Likelihoods with Applications to
1230 Phylogenetic Inference. Mol Biol Evol. 1999;16(8):1114-. doi:
1231 10.1093/oxfordjournals.molbev.a026201.

1232 121. Tajima F, Nei M. Estimation of evolutionary distance between nucleotide sequences. Mol Biol
1233 Evol. 1984;1(3):269-85. doi: 10.1093/oxfordjournals.molbev.a040317.

1234 122. Tamura K, Stecher G, Kumar S. MEGA11: Molecular Evolutionary Genetics Analysis Version
1235 11. Mol Biol Evol. 2021;38(7):3022-7. doi: 10.1093/molbev/msab120. PubMed PMID: 33892491.

1236 123. Bitinaite J, Nichols NM. DNA cloning and engineering by uracil excision. Curr Protoc Mol Biol.
1237 2009;Chapter 3:Unit 3 21. doi: 10.1002/0471142727.mb0321s86. PubMed PMID: 19343708.

1238 124. Nour-Eldin HH, Hansen BG, Norholm MH, Jensen JK, Halkier BA. Advancing uracil-excision
1239 based cloning towards an ideal technique for cloning PCR fragments. Nucleic Acids Res.
1240 2006;34(18):e122. doi: 10.1093/nar/gkl635. PubMed PMID: 17000637.

1241 125. Lampropoulos A, Sutikovic Z, Wenzl C, Maegele I, Lohmann JU, Forner J. GreenGate - A
1242 Novel, Versatile, and Efficient Cloning System for Plant Transgenesis. PLOS ONE.
1243 2013;8(12):e83043. doi: 10.1371/journal.pone.0083043.

1244 126. Tesei G, Lindorff-Larsen K. Improved predictions of phase behaviour of intrinsically
1245 disordered proteins by tuning the interaction range [version 2; peer review: 2 approved]. Open
1246 Research Europe. 2023;2(94). doi: 10.12688/openreseurope.14967.2.

1247 127. Dignon GL, Zheng W, Kim YC, Best RB, Mittal J. Sequence determinants of protein phase
1248 behavior from a coarse-grained model. PLOS Computational Biology. 2018;14(1):e1005941. doi:
1249 10.1371/journal.pcbi.1005941.

1250 128. Benayad Z, von Bülow S, Stelzl LS, Hummer G. Simulation of FUS Protein Condensates with
1251 an Adapted Coarse-Grained Model. Journal of Chemical Theory and Computation. 2021;17(1):525-
1252 37. doi: 10.1021/acs.jctc.0c01064.

1253 129. Kleinboelting N, Huep G, Kloetgen A, Viehoever P, Weisshaar B. GABI-Kat SimpleSearch:
1254 new features of the Arabidopsis thaliana T-DNA mutant database. Nucleic Acids Res.
1255 2012;40(Database issue):D1211-D5. Epub 2011/11/12. doi: 10.1093/nar/gkr1047. PubMed PMID:
1256 22080561.

1257 130. Robert X, Gouet P. Deciphering key features in protein structures with the new ENDscript
1258 server. Nucleic Acids Res. 2014;42(Web Server issue):W320-4. doi: 10.1093/nar/gku316. PubMed
1259 PMID: 24753421; PubMed Central PMCID: PMC4086106.

1260 131. Jurrus E, Engel D, Star K, Monson K, Brandi J, Felberg LE, et al. Improvements to the APBS
1261 biomolecular solvation software suite. Protein Sci. 2018;27(1):112-28. doi: 10.1002/pro.3280.

1262 132. Akdel M, Pires DEV, Pardo EP, Jänes J, Zalevsky AO, Mészáros B, et al. A structural biology
1263 community assessment of AlphaFold2 applications. Nat Struct Mol Biol. 2022;29(11):1056-67. doi:
1264 10.1038/s41594-022-00849-w.

1265 133. Paysan-Lafosse T, Blum M, Chuguransky S, Grego T, Pinto BL, Salazar Gustavo A, et al.
1266 InterPro in 2022. Nucleic Acids Res. 2023;51(D1):D418-D27. doi: 10.1093/nar/gkac993.

1267 134. Käll L, Krogh A, Sonnhammer ELL. A Combined Transmembrane Topology and Signal
1268 Peptide Prediction Method. Journal of Molecular Biology. 2004;338(5):1027-36. doi:
1269 10.1016/j.jmb.2004.03.016.

1270 135. Stecher G, Tamura K, Kumar S. Molecular Evolutionary Genetics Analysis (MEGA) for
1271 macOS. Mol Biol Evol. 2020;37(4):1237-9. doi: 10.1093/molbev/msz312.
1272

1273

Supporting information captions

S1 Appendix. Extended Materials and Methods.

S1 Table. Isoforms contained in cYTHDF constructs, and templates used for PCR.

S2 Table. Constructs and DNA Oligonucleotides. All sequences are 5' to 3'.

S1 Dataset. Protein Sequences. Amino acid sequences of proteins used in this study with their identifiers and taxonomic classification. Abbreviations of species names match with those used in Figs 1 and S1. For YTHDF proteins, the canonical YTH domain is colored in blue, and long internal insertions within the YTH domain are highlighted in a paler shade of blue. Additional folded domains are marked in other colors. The sequence of the IDR used for biophysical simulations of some of the proteins is the entire sequence upstream to the YTH domain. For the human fused in sarcoma (FUS) RNA-binding protein used as control for the analyses of IDR properties, the IDR sequence is highlighted in **bold**.

S2 Dataset. Full length alignment of Viridiplantae YTHDF proteins. Full-length amino acid sequence alignment of the YTHDF proteins used for the phylogenetic analyses in Figs 1 and S1. The alignment was obtained using MUSCLE (Multiple Sequence Comparison by Log-Expectation [112, 113]), and is given in clustal format.

S3 Dataset. Trimmed alignment of Viridiplantae YTHDF proteins. Amino acid sequence alignment of the YTHDF proteins used for the phylogenetic analyses in Figs 1 and S1 after trimming the poorly conserved regions (IDRs) at both ends, according to the score given by Jalview [114] (S23 Fig), from the alignment provided in S2 Dataset.

S4 Dataset. Phylogenetic tree of Viridiplantae YTHDF proteins. Phylogenetic tree (Maximum likelihood phylogenetic analysis) in Nexus/Newick format obtained from the trimmed alignment provided in S3 Dataset. Values of nodes are SH-aLRT (%) support.

S5 Dataset. Full length alignment of YTHDF proteins in Viridiplantae focused on early-diverging clades. Full-length amino acid sequence alignment of selected YTHDF proteins, with focus on early-diverging taxa within Viridiplantae, used for S3 and S4 Figs. The names of the proteins are preceded by a 'tag' related to the DF clade and organism taxon to facilitate a meaningful sorting of the alignment for illustration purposes. The alignment was obtained using MUSCLE (Multiple Sequence Comparison by Log-Expectation [112, 113]), and is given in clustal format.

S6 Dataset. Raw T1 complementation counts. Numerical data and calculations supporting the histograms in Figs 2C-D, 4B, 6B-C, and S7.

S7 Dataset. Full length alignment of YTHDF proteins for the calculation of evolutionary divergence of *Ath* ECTs. Full-length amino acid sequence alignment of 101 YTHDF proteins from selected taxa (bryophytes, basal angiosperms, magnoliids and dicots) used for pairwise comparisons to calculate evolutionary distances between *Mpo* DFE and *Ath* ECTs (S8 Dataset, Fig 6A). All the sequences with their identifiers and the taxonomic classification of the organisms can be found in S1 Dataset. The alignment was computed with MUSCLE (Multiple Sequence Comparison by Log-Expectation [112, 113]), and is given in clustal format.

S8 Dataset. Evolutionary divergence of *Ath* ECTs. Matrix with estimates of evolutionary divergence (number of amino acid substitutions per site) between 101 land plant proteins from selected taxa (bryophytes, basal angiosperms, magnoliids and dicots) according to the alignment in

S7 Dataset. The analysis was conducted using the Equal Input model [121] in MEGA11 [122, 135]. All positions containing gaps and missing data were eliminated (complete deletion option). There were a total of 171 positions in the final dataset. A complete matrix ('Matrix output') as well as a selection of the comparisons regarding *Ath* ECTs vs. *Mpo* DFE, is extracted from the matrix in a separate sheet ('Selection'). Color-coding follows the rest of the figures in the article. The graphic representation of the values is shown in Fig 6A.

S9 Dataset. Raw data and calculations supporting qPCR data in Fig 3H

S1 Movie. ECT2 simulation. Coarse-grained molecular dynamics simulation of 100 ECT2 IDRs using the CALVADOS 2 forcefield (7.5 microseconds simulation time) [126]. The proteins are colored differently to distinguish individual chains.

S2 Movie. ECT1 simulation. Coarse-grained molecular dynamics simulation of 100 ECT1 IDRs using the CALVADOS 2 forcefield (7.5 microseconds simulation time) [126]. The proteins are colored differently to distinguish individual chains.

S3 Movie. ECT11 simulation. Coarse-grained molecular dynamics simulation of 100 ECT11 IDRs using the CALVADOS 2 forcefield (7.5 microseconds simulation time) [126]. The proteins are colored differently to distinguish individual chains.